Cellular Signalling 62 (2019) 109340

Contents lists available at ScienceDirect

Cellular Signalling

journal homepage: www.elsevier.com/locate/cellsig

PICOT (GLRX3) is a positive regulator of stress-induced DNA-damage response☆

Pinakin Pandya, Alex Braiman, Noah Isakov*

The Shraga Segal Department of Microbiology, Immunology and Genetics, Faculty of Health Sciences and the Cancer Research Center, Ben Gurion University of the Negev, P.O.B. 653, Beer Sheva 84105, Israel.

ARTICLE INFO

Keywords:
PICOT
GLRX3
H2AX
DNA-damage response
Genotoxic stress

ABSTRACT

Protein kinase C (PKC)-interacting cousin of thioredoxin (PICOT; also termed glutaredoxin 3 (Glrx3)) is a ubiquitously expressed protein that possesses an N-terminal monothiol thioredoxin (Trx) domain and two C-terminal tandem copies of a monothiol Glrx domain. It has an overall highly conserved amino acid sequence and is encoded by a unique gene, both in humans and mice, without having other functional gene homologs in the entire genome. *Despite* being *discovered almost* two decades *ago,* the biological function of *PICOT* remains largely ill-defined and its ramifications are underestimated considering the fact that PICOT-deficiency in mice results in embryonic lethality.

Since classical Glrxs are important regulators of the cellular *redox homeostasis, we tested* whether PICOT participate in the stress-induced DNA-damage response, focusing on nuclear proteins that function as integral components of the *DNA repair* machinery. Using wild type versus PICOT-deficient (PICOT-KD) Jurkat T cells we found that the anti-oxidant mechanism in PICOT-deficient cells is impaired, and that these cells respond to genotoxic drugs, such as etoposide and camptothecin, by increased caspase-3 activity, a reduced survival and a slower and diminished phosphorylation of the histone protein, H2AX. Nevertheless, the effect of PICOT on the drug-induced phosphorylation of H2AX was independent of the cellular levels of reactive oxygen species. PICOT-deficient cells also demonstrated reduced and slower γH2AX foci formation in response to radiation. Furthermore, immunofluorescence staining using PICOT- and γH2AX-specific Abs followed by confocal microscopy demonstrated partial localization of PICOT at the γH2AX-containing foci at the site of the DNA double strand breaks. In addition, PICOT knockdown resulted in inhibition of phosphorylation of ATR, Chk1 and Chk2 kinases, which play an essential role in the DNA-damage response and serve as upstream regulators of γH2AX. The present data suggest that PICOT protects cells from DNA damage-inducing agents by operating as an upstream positive regulator of ATR-dependent signaling pathways. By promoting the activity of ATR, PICOT indirectly regulates the phosphorylation and activation of Chk1, Chk2, and γH2AX, which are critical components of the DNA damage repair mechanism and thereby attenuate the stress- and replication-induced genome instability.

1. Introduction

Reactive oxygen species (ROS) are routinely produced as by-products of the normal metabolism and oxidative phosphorylation of normal cells. They include molecules such as superoxide (O_2-), hydrogen peroxide (H_2O_2) and hydroxyl ions (OH), and when generated under regulated physiological conditions, they play important roles in cellular signaling and homeostasis [1,2]. For example, ROS participate in signaling pathways regulating cell cycle progression and proliferation, cell migration and differentiation, as well as inflammation and other immune cell functions [3–6].

Nevertheless, the production of excessive ROS triggered by *environmental stressors,* such as ionizing radiation, ultraviolet light, or chemotherapeutic drugs [7–9], may cause severe damages to cellular components, especially the DNA, and induce single and/or double-strand breaks that may result in cell death and tissue destruction

☆ This work was funded in part by the USA-Israel Binational Science Foundation (grant no. 2013034) and the Israel Science Foundation administered by the Israel Academy of Science and Humanities (grant no. 1235/17). N.I. holds the Joseph H. Krupp Chair in Cancer Immunobiology.

* Corresponding author at: The Shraga Segal Department of Microbiology, Immunology and Genetics, Faculty of Health Sciences, Ben-Gurion University, Beer-Sheva, Israel.

E-mail address: noah@bgu.ac.il (N. Isakov).

https://doi.org/10.1016/j.cellsig.2019.06.005
Received 7 April 2019; Received in revised form 15 May 2019; Accepted 4 June 2019
Available online 05 June 2019

[10–13].

To prevent the harmful effects of these oxidative challenges, aerobic organisms developed an array of defense strategies that rely on endogenous non-enzymatic and enzymatic antioxidants. The first group includes free radical scavengers such as vitamin C and E, glutathione and uric acid [14], while the second comprises catalases, superoxide dismutases, and glutathione peroxidases and reductases [15].

Thioredoxins (Trxs) and glutaredoxins (Glrxs) are two additional groups of redox-regulating enzymes which promote protein reduction by cysteine thiol-disulfide exchange and contribute to the maintenance of redox homeostasis in living cells [16,17]. The mammalian Glrxs are grouped into two major subfamilies. The classical Glrxs are small ubiquitous glutathione (GSH)-dependent oxidoreductases that possess a Cys-Pro-Tyr-Cys (CPYC) motif in their active site and catalyze the reversible reduction of protein disulfide bridges or protein-GSH mixed disulfide bonds [18]. The second group includes the monothiol Glrxs that contain a single cysteine residue in their active-site (usually, a Cys-Gly-Phe-Ser (CGFS) motif), are ubiquitously expressed and found in all branches of the evolutionary tree [19,20].

While monothiol Glrxs in prokaryotes and eukaryotes are composed of a CGFS signature-containing active site within a single domain, eukaryotes possess additional multidomain CGFS signature-containing monothiol Glrxs, that include a single N-terminal monothiol Trx domain and one or more C-terminal monothiol Glrx domains [19,21,22].

The first mammalian monothiol Glrx was discovered in T lymphocytes during a search for protein kinase C (PKC)-binding partners [23]. Based on its structural similarity to Trx ability to interact with PKC this newly discovered protein was termed PKC-interacting cousin of thioredoxin, abbreviated as PICOT (also known as TXNL2, Grx3 and Glrx3).

PICOT is a ubiquitous protein which possesses an N-terminal monothiol Trx domain followed by a tandem repeat of monothiol Glrx domains (also termed PICOT homology domains) [19]. It is critical for embryogenesis since PICOT-deficient mouse embryos die towards the end of the second trimester of pregnancy [24,25]. Several independent studies demonstrated the involvement of PICOT in signal regulation in different cell types [23,25,26] and supported some ill-defined regulatory functions of PICOT in T lymphocyte responses [23], cardiac hypertrophy [25,27], and proliferation of various types of normal and transformed cells [24,28–31].

We found that the PICOT protein undergoes tyrosine phosphorylation and nuclear translocation in response of T lymphocytes to hydrogen peroxide [32,33], and predicted a potential role for PICOT in cellular responses to ROS.

Experiments performed in HeLa cells and mouse fibroblasts reconfirmed that oxidative stress promotes PICOT translocation into the nucleus and further demonstrated that this recruitment is reversible in a redox-dependent manner [34]. In addition, low levels of PICOT rendered cells susceptible to oxidative stress, whereas overexpressed nuclear-targeted PICOT protected cells from oxidative stress [34].

In vivo studies revealed that PICOT mRNA was induced during oxidative stress [24], and that PICOT was able to alleviate myocardial ischemia-reperfusion injury by regulating intracellular ROS and free iron levels [35].

A role for PICOT in cellular iron homeostasis was further demonstrated by showing that PICOT homodimers and PICOT-BolA2 heterodimers operate as iron-sulfur cluster chaperones that can transfer [2Fe−2S] clusters to [2Fe-2S]-dependent enzymes [36–39]. PICOT deficiency in HeLa cells led to decreased activities of several cytosolic Fe/S proteins, which resulted in the downregulation of ferritin levels and increased expression of transferrin receptors [38]. Since PICOT-$[2Fe{-}2S]^{2+}$ clusters, which are not redox active, dissociate in the presence of ferricyanide or S-nitroso glutathione, it has been suggested that the redox-induced dissociation of PICOT-$[2Fe{-}2S]^{2+}$ clusters serves as a cellular mechanism for activation of PICOT in response to reactive oxygen and nitrogen species [36].

In the present study we further tested the role of PICOT in the stress-induced DNA-damage response, focusing on nuclear proteins that regulate and/or execute this DNA damage response. We found that PICOT knockdown led to increased intracellular ROS in hydrogen peroxide-treated Jurkat T cells. In addition, following treatment with genotoxic drugs, PICOT-deficient cells exhibited increased levels of active caspase-3 and decreased survival. Nevertheless, the effect of PICOT on the formation of γH2AX was ROS independent. PICOT-deficient cells also exhibited a delayed and reduced phosphorylation of H2AX in response to drug or irradiation. In addition, partial colocalization of PICOT with the γH2AX-containing foci was observed at the double strand DNA-breaks. Finally, PICOT knockdown resulted in inhibition of phosphorylation of the H2AX-upstream kinases, supporting a positive role for PICOT in the regulation of very early events of the stress-induced DNA-damage response.

2. Materials and methods

2.1. Reagents and antibodies

Hydrogen peroxide (H_2O_2), Camptothecin, 3-(4, 5-dimethylthiazol-2-yl)-2,5-diphenyltetrazolium bromide (MTT) and 2′-7′-Dichloro-Dihydro-Fluorescein Diacetate (DCFH-DA) were from Sigma-Aldrich, Israel. Etoposide was from EBEWE Pharma, Austria. A mouse monoclonal antibody (mAb) specific for PICOT was from Santa Cruz Biotechnology, Inc. (Santa Cruz, CA) and a mAb anti-β-actin was from Merck Millipore (Darmstadt, Germany). Rabbit polyclonal antibodies specific for H2AX, ATR, phospho-Ser-139 of H2AX (γH2AX), and mouse mAb anti-Chk1 were from Abcam Biotechnology Company (Cambridge, UK). Rabbit polyclonal antibodies anti-phospho-Ser-1981 ATM, phospho-Ser-428-ATR, phospho-Ser-345-Chk1 and phospho-Thr-68-Chk2 were from Cell Signaling Technology Inc. (Danvers, MA). Cyanine3 (Cy3)-conjugated goat anti-mouse IgG and Cyanine5 (Cy5)-conjugated goat anti-rabbit IgG were from *Jackson ImmunoResearch* Laboratories, *Inc*. (*West Grove, P*A) and Kirkegaard & Perry Laboratories (KPL; Gaithersburg, MD), respectively. DAPI was from Biotium, Inc. (Hayward, CA). Horseradish peroxidase (HRP)-conjugated goat anti-mouse and goat anti-rabbit immunoglobulin Abs were from Abcam Biotechnology.

2.2. Cell lines and culture condition

The Jurkat human T-cell line (clone E6-1; ATCC® TIB-152™), PICOT-deficient Jurkat-derived cell lines (1A, 2G) and control scrambled plasmid sc-PICOT-expressing Jurkat-derived cell line (5A) were maintained at a logarithmic growth phase in complete RPMI (RPMI 1640 supplemented with 10% heat-inactivated fetal calf serum (FCS), 2 mM L-glutamine, 50 units/ml penicillin, 50 μg/ml streptomycin (all from Biological Industries, Beit Haemek, Israel), and 0.5 μM β-mercaptoethanol (Sigma)).

2.3. Preparation of PICOT-deficient Jurkat T cells

PICOT shRNA plasmids were designed and synthesized by SuperArray Bioscience (Frederick, MD) and cloned into an expression vector (pGeneClip) that directs the synthesis of small hairpin RNAs (shRNAs) in mammalian cells, under the control of the polymerase III promoter, and contain the neomycin resistance gene for selection of stably transfected cells. We used a set of four sense strands of 21 nucleotide sequences of human PICOT (CCAACATACCCTCAGCTGTAT; CTACCCAGCGCTAATGAACAT; GTGGAAATTCTTCACAAACAT; ACTC CCTCAAGTTTC ATTTGT), plus a control scrambled sequence. The sense strand was followed by a 10-nucleotide spacer (CTTCCTGTCA) and reverse complement of the same 21 nucleotide sequence. After cloning these short sequences downstream of the U1 promoter of the plasmid, the resulting pGeneClip-PICOT-shRNA plasmids were transfected into Jurkat E.6 cells by electroporation using a BioRad Gene

Pulser. G418 resistant stable transfectants were isolated and cloned and their PICOT expression levels were determined by Western blot and qRT-PCR.

2.4. Cell irradiation

Jurkat T cells were irradiated with X-rays at a dose of 2 Gy (1.3 Gy/min, 160 kV, 25 mA) using the Ben Gurion University RAD Source RS-2000 (Biological system) X-ray cabinet. Cell irradiation was performed at room temperature with cells kept submerged in 3 ml of warmed culture medium. Pre- and post-irradiation, cells were kept in a 37 °C, 5% CO_2 incubator. Control treatments were performed using the same protocol with no irradiation.

2.5. MTT cell viability assay

The *MTT assay* is a colorimetric assay for assessing cell metabolic activity which correlates with the number of *viable* cells present [40]. It is based on the ability of viable cells to reduce the yellow tetrazole, MTT (3-(4, 5-dimethyl)-2, 5-diphenyl tetrazolium bromide) to a blue formazan product. Cells (4×10^4/well in 96-well microtiter plates) were treated with different concentrations of H_2O_2 (30 min) or etoposide (8 h) at 37 °C in a 5% CO_2-incubator. Cells were then washed with PBS and incubated with 25 μl of MTT solution (5 mg/ml in PBS) for 2 h at 37 °C. Reactions were terminated by the addition of 100 μl/well of stop buffer (SDS 20%, DMFA, acetic acid 80%, HCl 1 N), which dissolved the resultant formazan crystals. Samples were kept overnight, and the absorbance intensity was quantified using an ELISA microplate reader (Bio-RAD 680, USA) at 490 nm, with a reference wavelength of 620 nm. All experiments were performed in triplicates and the relative cell viability was calculated as a percentage relative to the results of untreated cells, using the formula:

$$\text{(Viable cells) } \% = 100 \times \text{(absorbance of } H_2O_2 \text{or etoposide treated cells /absorbance of untreated cells).}$$

2.6. In vitro ROS measurement

Intracellular ROS formation was measured using the oxidant-sensing fluorescent probe 2′-7′-Dichloro-dihydro-fluorescein Diacetate (DCFH-DA) (Sigma, St. Louis, MO), as described [41]. DCFH-DA is a nonpolar dye that converts into a polar derivative, DCFH, by cellular esterases that are non-fluorescent and switched to highly fluorescent DCF when oxidized by intracellular ROS and other peroxides. Cells (4×10^4/well) were seeded onto wells of 96-well plates (black/clear bottom, BD Biosciences, San Jose, CA) for an overnight incubation. Samples were then treated with different concentrations of H_2O_2 for 30 min at 37 °C in a 5% CO_2-incubator. The wells were then washed twice with PBS followed by the addition of 10 μM DCFH-DA (diluted in 100 μl complete RPMI with 5% FCS) for 60 min at 37 °C, in a 5% CO_2-incubator. The extent of fluorescence was measured using a fluorescence microplate reader (TECAN Infinite, Mannedorf, Switzerland) at fluorescence excitation and emission wavelengths of 485 and 525 nm, respectively.

2.7. Analysis of DNA fragmentation

Jurkat and Jurkat.1A cells (5×10^5/ml) were treated with etoposide or camptothecin at 37 °C in a 5% CO_2-incubator. Cells were then collected, washed in cold PBS and gently re-suspended in 0.5 ml of lysis buffer (10 mM Tris-HCl, pH 7.4, 1 mM EDTA (Tris-EDTA; TE) and 10% Triton X-100). The cell suspension was incubated for 30 min at room temperature and centrifuged at 12,000 RPM for 30 min. The DNA-containing supernatant was transferred to a new Eppendorf tube and precipitated by the addition of 150 μl NaCl (5 M) and 500 μl ethanol, for 1 h at −80 °C. Samples were then centrifuged at 12,000 RPM for 30 min and supernatants were removed, followed by the addition of 1 ml of 70% ethanol to the DNA pellet. The samples were centrifuged once more at 12,000 RPM for 15 min, supernatants were removed, and DNA samples were then dissolved in TE buffer and treated with RNase (5 mg/ml) for 1 h at 37 °C. The resulted DNA-containing solution was quantitated spectrophotometrically at 260/280 nm, mixed with loading buffer, and fractionated on a 1.5% agarose gel containing 0.45 μg/ml ethidium bromide. After electrophoresis, gels were illuminated with ultraviolet light for examination and photography.

2.8. Detection of cleaved caspase-3-positive cells in live cells

Detection of cleaved caspase-3 was performed in live cells using NucView® 488 caspase-3 assay kit (Biotium, Inc., Fremont, CA). Jurkat and Jurkat.1A cells (2×10^6/group) were either untreated or treated with 10 μM etoposide for the indicated time points at 37 °C in a 5% CO_2-incubator. Cells were then centrifuged and cell pellets were treated according to the manufacturer's instructions. Caspase-3-positive cells were analysed using flow cytometer (BD FACSCanto™ II Flow cytometer). Ten thousand cells/group were screened and the percentage of caspase-3 positive cells out of the total number of live cells was calculated and presented as a bar graph. Images were taken using an Olympus Fluoview 1000 laser scanning confocal microscope.

2.9. Preparation of whole cell lysates and cytoplasm and nuclei fractions

Whole cell lysates were prepared by re-suspension of cells in lysis buffer (25 mM Tris-HCl, pH 7.5, 150 mM NaCl, 5 mM EDTA, 1 mM Na_3VO_4, 50 mM NaF, 10 μg/ml each of leupeptin and aprotinin, 2 mM AEBSF and 1% Triton X-100), and incubation (30 min) on ice. Lysates were centrifuged at 13,000 rpm for 30 min at 4 °C and the supernatants were collected as whole cell lysate.

Nuclear extracts were prepared as described [42]. Cells were re-suspended in buffer A (10 mM Tris-HCl, pH 7.4, 10 mM NaCl and 1 mM EDTA) plus a mixture of protease inhibitors (2 μg/ml aprotinin, 2 μg/ml leupeptin, 1 μg/ml pepstatin A, 2 μg/ml antipain, and 100 μg/ml PMSF) and kept on ice for 15 min. Samples were homogenized by passing through a 21G needle (15 times), and cytosolic fractions (supernatants) were obtained by 10 min centrifugation at 13,000 rpm at 4 °C. The pellets were resuspended in buffer B (10 mM Tris-HCl, pH -7.4, 10 mM NaCl and 1.5 mM $MgCl_2$ supplemented with a mixture of protease inhibitors (as above) plus 1 M (final concentration) NaCl, followed by 30 min incubation on ice. The samples were centrifuged for 10 min at 13,000 rpm and 4 °C in a microcentrifuge tube and the supernatants were collected and designated as nuclear extract. Total protein concentration was determined using the Bio-Rad protein assay kit. Aliquots of the extracts were stored at −20 °C.

2.10. Electrophoresis and immunoblotting

Whole cell lysates and cellular fractions were resolved by electrophoresis on 10% or 12.5% polyacrylamide gels using Bio-Rad Mini-PROTEAN II cells. Proteins from the gel were electroblotted onto nitrocellulose membranes (Schleicher and Schuell) at 100 V for 1 h, using BioRad Mini Trans-Blot transfer cells. After 1 h of blocking with 3% BSA in PBS at 37 °C, the nitrocellulose membranes were incubated with the indicated primary Abs, followed by incubation with HRP-conjugated goat anti-mouse or goat anti-rabbit IgG. Immunoreactive protein bands were visualized using an ECL reagent and autoradiography.

2.11. Cell staining and confocal microscopy

For irradiation studies, Jurkat and Jurkat.1A T cells (2×10^6/group) were irradiated (X-ray, 2 Gy) and left to recover for the indicated time points in vitro at 37 °C in a 5% CO_2 incubator. The cells were then

seeded on poly-L-lysine-coated 8 well μ-slide (ibidi Ltd.) and deposited on the slides by centrifugation at 1200 rpm for 5 min. Then, cells were fixed in 4% paraformaldehyde (Sigma)/PBS for 15 min at room temperature, permeabilized with PBS/0.2% Triton X-100 for 5 min and incubated with mouse anti-PICOT and rabbit anti-γH2AX Abs in a blocking buffer (PBS containing 1% BSA) for 1 h at room temperature. After three washes in PBS, the cells were incubated with Cy3-conjugated goat anti-mouse Ig Abs (1:500), Cy5-conjugated goat anti-rabbit Ig Abs (1:500), and DAPI (1 μg/ml) in PBS for 1 h at room temperature in the dark. Confocal microscopy analysis was performed on Olympus Fluoview 1000 laser scanning confocal microscope.

Quantification of the green (PICOT) and red (γH2AX) fluorescence colocalization was assessed by calculating the *correlation coefficient* on ~100 cells per condition using the *JACoP* plugin on *ImageJ* [43]. The Manders' coefficient values after threshhold setting are shown. M1 represents the fraction of green overlapping red and M2 value shows fraction of red overlapping green.

For γH2AX foci quantification, the total number of nuclei and foci in ~5 arbitrarily selected microscopic fields were calculated using the Image J software and the average number of γH2AX foci per nucleus was determined. The statistical significance of the differences between Jurkat and Jurkat.1A cells was determined using the *t*-test with the help of GraphPad software Prism5 (GraphPad, La Jolla/CA, USA).

3. Results

3.1. Knock-down of PICOT in Jurkat T cells reduces cell survival, increases intracellular ROS levels and promotes DNA fragmentation in response to ROS-inducing agents

Based on its primary amino acid sequence and overall structure, PICOT was assigned to the Glrx family, and although little is known regarding its catalytic activity, indirect studies suggest a role for PICOT in the regulation of intracellular redox homeostasis.

To analyse the potential involvement of PICOT in T cell resistance to ROS-inducing stress conditions, we compared the effect of hydrogen peroxide (H_2O_2) and etoposide treatment on the viability of Jurkat T cells vs. Jurkat.1A T cells, which express lower levels of PICOT due to constitutive expression of PICOT-shRNA (Fig. 1A). Cells were cultured in wells of 96-well plates in the presence of the indicated concentration H_2O_2 or etoposide and their viability was evaluated using the MTT assay, which measures the ability of live cells to reduce MTT to a blue formazan product. Cells viability in response to H_2O_2 (Fig. 1B) and etoposide (Fig. 1C) was reduced in a concentration dependent manner, and PICOT-deficient Jurkat.1A cells exhibited higher sensitivity to drug treatment. The increase in the susceptibility of Jurkat.1A cells to drug treatment correlated with an increase in intracellular ROS levels following cell treatment with hydrogen peroxide (Fig. 1D). We then compared the susceptibility of Jurkat vs. Jurkat.1A cells to topoisomerase inhibitors, etoposide and camptothecin - two genotoxic drugs that cause single and double-strand DNA breaks, leading to chromosomal DNA fragmentation [44–46]. Both drugs were found to induce DNA fragmentation in a time and concentration dependent manner but responses of the two cell types were quantitatively and qualitatively different (Fig. 1E-G). Only very large DNA fragments, which serve as early markers of T cell commitment to apoptosis [47] were detected in Jurkat cells, compared to a DNA 'ladder' in Jurkat.1A cells, representing integer multiples of ~200 bp oligonucleosomal size fragments. The results suggest that PICOT plays a role in cellular mechanisms that counteract stress-induced damages and increases cell survival under stress conditions.

3.2. Knockdown of PICOT upregulates caspase-3 activity in etoposide-treated Jurkat T cells

To further analyse the potential role of PICOT in the genotoxic stress-induced DNA damage response, we tested the effect of PICOT deficiency on the activation state of caspase-3, a cysteine-aspartic acid protease that serves as a crucial mediator of programmed cell death [48]. The caspase-3 proenzyme is inactive in healthy cells but undergoes proteolytic cleavage in apoptotic cells into two subunits which dimerize and form an active enzyme. In the presence of the cell membrane-permeable NucView® 488 fluorogenic caspase substrate, cells with an active caspase-3 become fluorescent and their frequency can be determined.

In this assay, Jurkat and Jurkat.1A cells were treated with etoposide and then with the DEVD-NucView 488 caspase-3 substrate, followed by FACS analysis and confocal microscopy. The results demonstrate a direct correlation between the time of incubation with etoposide and the increase in the frequency and intensity of caspase-3 positive fluorescent cells (Fig. 2A and B). Furthermore, the frequency of caspase-3 positive cells was significantly higher in PICOT-deficient Jurkat.1A cells, both at 7 and 10 h post etoposide treatment. These results support the initial observations indicating that PICOT plays a positive role in cell protection from etoposide-induced cell death.

3.3. Knockdown of PICOT results in decreased and delayed expression of γH2AX in drug-treated and X-ray irradiated Jurkat T cells

The camptothecin and etoposide are chemotherapeutic agents that target DNA topoisomerase I and II, respectively, and are commonly used drugs in cancer treatment. Both drugs promote single and/or double-strand breaks (DSB) in the DNA, which promote the phosphorylation of the histone variant, H2AX (denoted as γH2AX) on Ser-139 [49]. In turn, γH2AX, which is critical for the maintenance of genome stability, promotes the assembly of the DNA repair proteins at the damaged sites and regulates the activation of checkpoint proteins which arrest the cell cycle progression.

Since the induction of γH2AX directly correlates with the detection of DSBs by the cell's sensing machinery and the initiation of the DNA damage response (DDR) [50], we tested whether PICOT knock down can influence the DNA repair mechanisms by evaluating the effect of PICOT on the intensity and/or time kinetic of phosphorylation of H2AX.

These studies were performed on wild type Jurkat T cells, PICOT-deficient Jurkat sublines that constitutively express sh-PICOT, and Jurkat sublines that constitutively express a control, scrambled sc-PICOT DNA. The cells were initially treated with etoposide for different time intervals and expression of γH2AX, compared to that of the non-phosphorylated H2AX, was determined using Western blot analysis. The results (Fig. 3A) demonstrated a gradual time-kinetic increase in γH2AX expression levels following etoposide treatment of Jurkat T cells. An increase of > 8-fold was observed at 10 h post-etoposide treatment. A much slower time kinetic of γH2AX expression was observed in PICOT-deficient Jurkat.1A cells, where the peak response at 10 h post etoposide treatment was ~2-fold lower than that of the wild type Jurkat T cells. The time-kinetic of γH2AX expression levels in Jurkat.5a which express scrambled sc-PICOT DNA and normal levels of PICOT, were similar to those observed in wild type Jurkat.

Immunoblot of the non-phosphorylated form of H2AX showed similar levels of protein expression in the three cell lines at all time points (Fig. 3B). The reduced levels of PICOT in Jurkat.1A are demonstrated in Fig. 3C and D, and expression of β-actin (Fig. 3D) serve to validate usage of equal amounts of proteins per lane. The relative changes in γH2AX vs. H2AX expression were quantifying by densitometry of the corresponding protein bands and normalization to those of β-actin protein bands (Fig. 3E).

We further tested the effect of camptothecin, a DNA topoisomerase I inhibitor, on γH2AX expression in Jurkat T cells and once again determined that drug treatment increased γH2AX expression by > 2-fold (Fig. 3F). In contrast, levels of γH2AX in Jurkat.1A and Jurkat.2G sublines, which express low levels of PICOT, were barely detectable in both untreated and camptothecin-treated cells (Fig. 3F). Immunoblot of

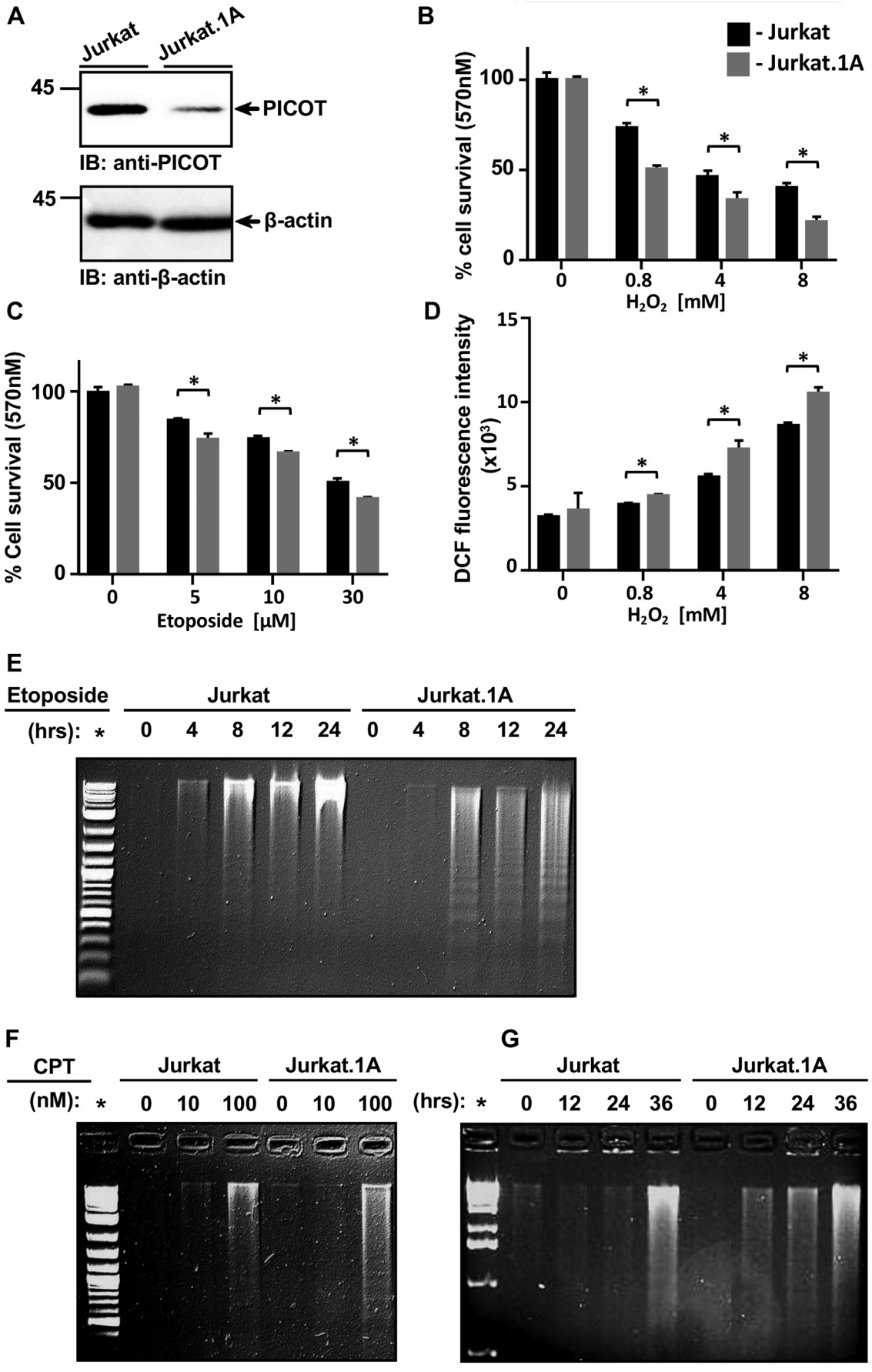

(caption on next page)

Fig. 1. Knockdown of PICOT decreases Jurkat-T cell resistance to genotoxic agents.
A. Whole cell lysates (20 μg proteins/lane) of wild-type Jurkat and Jurkat that constitutively express sh-PICOT (Jurkat.1A) were resolved by SDS-PAGE on 12.5% gels followed by protein electroblotting onto nitrocellulose membranes that were incubated with mouse anti-PICOT Abs followed by washing and a second incubation with an HRP-conjugated goat anti-rabbit Ig Abs. Membranes were then treated with immunoperoxidase ECL detection system followed by autoradiography. A parallel membrane was immunoblotted with β-actin Abs and served to validate the equal loading of proteins per lane. B and C. Jurkat and Jurkat.1A T cells were cultured in wells of 96-well plates (4×10^4 cells/well) in the presence of the indicated concentrations of H_2O_2 (30 min) or etoposide (7 h) at 37 °C, in a 5% CO_2 incubator. The cells' ability to reduce MTT to a blue formazan was measured, as an indication for the relative cell viability, and expressed as a percentage of the response of control cells (UT, untreated) D. Jurkat and Jurkat.1A T cells that were treated with H_2O_2 (30 min) were incubated with the fluorescence indicator DCFH-DA for 60 min and intracellular ROS levels were measured by fluorescence microplate reader. *E*-G. Jurkat and Jurkat.1A cells were treated with etoposide (E. 30 μM) or camptothecin for the indicated concentrations (F; 12 h), or time intervals (G. 100 nM), at 37 °C in a 5% CO_2 incubator. The relative fragmentation of DNA, as a hallmark of apoptosis, was measured by agarose gel electrophoresis of DNA samples isolated from the treated cells, followed by *ethidium bromide* staining. ROS, Reactive oxygen species; DCFH-DA, 2′-7′-Dichloro-Dihydro-Fluorescein-Diacetate; DCF, 2′-7′-Dichloro-Fluorescein. The data represent the mean ± SD of triplicate samples. *$P < .05$. The standard DNA ladder samples in panels D-F are marked with an asterisk (*).

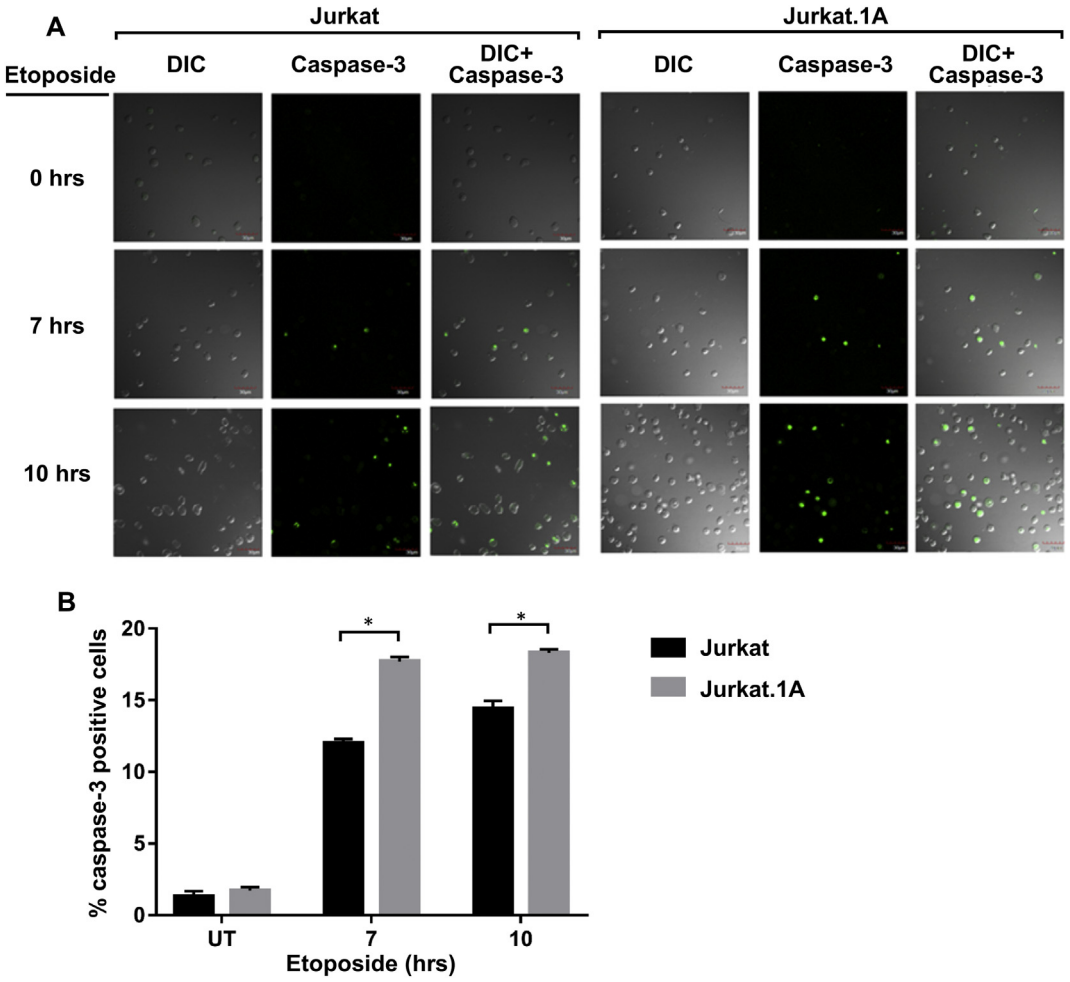

Fig. 2. Silencing PICOT results in increased caspase-3 activity in etoposide-treated Jurkat cells.
Jurkat and Jurkat.1A cells were treated with etoposide (10 μM) for the indicated time points and caspase-3 activity in live cell was detected using NucView® 488 caspase-3 assay kit. Cells were then analysed using confocal laser microscopy (A) and flow cytometry (B). The bar graph represents averages of caspase-3 positive live cells ± SD of duplicate samples (* P < .05), and the results are representative of three independent experiments. DIC, Differential interference contrast.

H2AX (Fig. 3G) demonstrated similar protein expression levels in all cell lines tested, with no effect of the camptothecin on H2AX protein expression. Immunoblot of β-actin confirmed that equal amounts of proteins were loaded per lane (Fig. 3H and I).

We then compared the kinetic of γH2AX foci formation in Jurkat and Jurkat.1A cells in response to X-ray irradiation. The cells were treated with 2 Gy X-ray and kept in an incubator for the indicated time points. Formation of discrete nuclear γH2AX foci post-irradiation were determined by fluorescent staining using anti-γH2AX Abs and cell analysis by confocal microscopy. A relatively weak staining of γH2AX was observed in resting Jurkat and Jurkat.1A cells (Fig. 4A, control cells). A relatively small number of γH2AX foci was observed in Jurkat T cells at 0.5 h post irradiation (Fig. 4A) and the number of foci increased and reached a maximal value at 1 h post irradiation. In contrast, the smaller number of γH2AX foci in Jurkat.1A cells was observed for 0.5 and 1 h time points and the time kinetics of γH2AX foci formation was delayed (Fig. 4A & 4B).

3.4. The PICOT protein partially colocalizes with γH2AX nuclear foci in irradiated Jurkat T cells

Cellular stress leading to double-strand DNA breaks (DSB) promotes

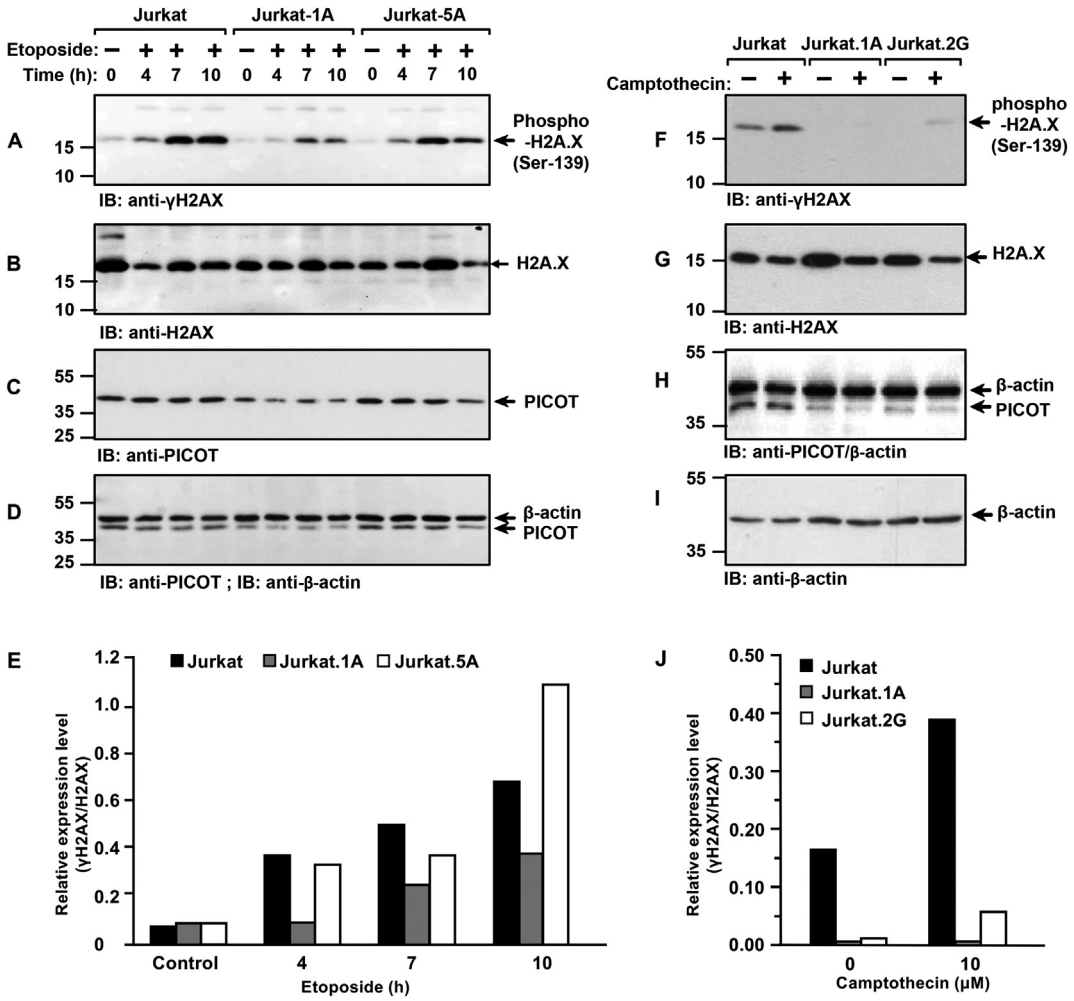

Fig. 3. PICOT knockdown in Jurkat T cells leads to a reduced and delayed expression of phospho-H2AX-Ser139 (γH2AX) in response to etoposide and camptothecin. Wild-type Jurkat, Jurkat that constitutively express sh-PICOT (sublines 1A and 2G) and Jurkat that express the control scrambled plasmid sc-PICOT (subline 5A) (5×10^6/group) were treated with etoposide (10 μM) for indicated time intervals at 37 °C in a 5% CO_2 incubator (A-E), or with camptothecin (10 μM) for 1 h (F-J). Whole cell lysates (20 μg proteins/lane) were then resolved by SDS-PAGE on 12.5% gels followed by protein electroblotting onto nitrocellulose membranes. Phospho-H2AX (γH2AX) was visualized by membrane incubation with rabbit polyclonal anti-γH2AX Abs followed by washing and a second incubation with an HRP-conjugated goat anti-rabbit Ig Abs. Membranes were then treated with immunoperoxidase ECL detection system followed by autoradiography (A, F). The membranes were then stripped and immunoblotted with Abs specific for H2AX (B, G). Immunoblot of PICOT (C, D, H) served to demonstrate the extent of the reduction in its expression in the sh-PICOT expressing lines, while immunoblot of β-actin (D, H, I) served to validate the equal loading of proteins per lane. The intensity of the indicated protein band signals was determined by *ImageJ* software and the values of γH2AX divided by H2AX are presented as a bar graph (E, J). Molecular size markers (in kDa, kilodaltons) are indicated on the left. The position of specific protein bands is indicated by arrows. Results are representative of three independent experiments. IB, Immunoblot.

the phosphorylation of H2AX and formation of discrete γH2AX-containing *foci* at the DNA damage *sites* [51]. We found that drugs, such as etoposide, and irradiation induced higher expression levels of γH2AX, which were correlated with the expression levels of PICOT. Since the γH2AX-containing foci serve as platforms for the recruitment of chromatin modifying proteins, we tested whether PICOT colocalizes with γH2AX within these foci. Staining of control cells revealed a relatively weak expression of γH2AX in the cytoplasm and nuclei of Jurkat T cells (Fig. 5, control). Stronger staining of γH2AX was observed in cells at 30 min post-irradiation, where staining was observed as discrete nuclear foci (Fig. 5, 0.5 h).

PICOT staining in the cytoplasm of untreated cells was slightly brighter than in the nucleus, and irradiation had only a modest effect on its subcellular distribution or intensity (Fig. 5). An overlay pictures of PICOT and γH2AX staining demonstrated partial colocalization of PICOT and γH2AX at 1 and 2 h post irradiation (Fig. 5).

The *Pearson's correlation coefficients* (P) and the Mander's overlap coefficients that were used for quantifying the degree of colocalization of green (PICOT) and red (γH2AX) fluorescence (using the *JACoP ImageJ* plugin [43], indicated that the basal P values in control cells increased gradually with the time post irradiation, from a P values of 0.136 ± 0.02 at 0.5 h post irradiation to a *P* value of 0.278 ± 0.02 at 2 h post irradiation.

The results suggest that the irradiation-induced PICOT colocalization within the γH2AX foci might indirectly alter the extent of phosphorylation and activation of H2AX and thereby modulating DNA repair mechanisms.

3.5. Knockdown of PICOT results in decreased and delayed expression of nuclear γH2AX in camptothecin- and etoposide-treated Jurkat T cells

Our studies demonstrating that the γH2AX expression levels positively correlate with PICOT expression were performed using whole cell lysates, and since γH2AX predominates in cell nuclei, we further tested whether such a correlation exists in the nuclear compartment.

Jurkat and PICOT-deficient Jurkat.1A cells were treated with

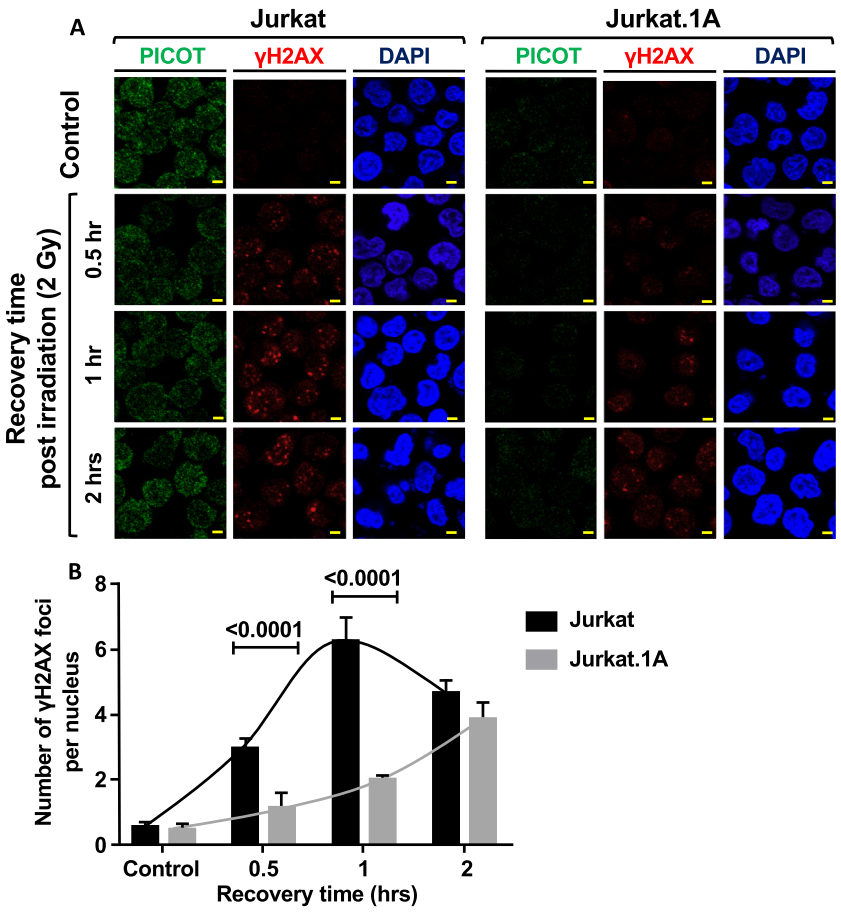

Fig. 4. Knockdown of PICOT results in a reduced and delayed formation of γH2AX foci in irradiated Jurkat T cells.
A. Jurkat and Jurkat.1A cells (2×10^6/group) were irradiated with X-ray (2 Gy) and left to recover in vitro for the indicated time points at 37 °C in a 5% CO_2 incubator. The cells were then seeded on poly-L-lysine-coated slides and deposited by centrifugation. After fixation and permeabilization, the cells were incubated with mouse anti-PICOT and rabbit anti-γH2AX Abs, followed by staining with Cy3 (green)-conjugated goat anti-mouse and Cy5 (red)-conjugated goat anti-rabbit Ig Abs plus DAPI (blue). Cells were then analysed on an Olympus Fluoview 1000 laser scanning confocal microscope. Control treatments were performed using the same protocol with no irradiation. Scale bar equals 2.5 μM. B. Quantification of γH2AX foci in individual cells was calculated in five different image fields using the Image J software. Each bar represents the average number of foci/cell number ± standard deviation ($n = 50$). The level of significance was determined using the *t*-test and obtained *p* values are indicated.

etoposide for different time intervals or with different concentrations of camptothecin, fractionated into cytosolic and nuclear fractions which were then separated by standard SDS-PAGE and immunoblotted with anti-γH2AX Abs.

The results demonstrated that the levels of γH2AX in untreated cells were almost undetectable (Fig. 6A, F), and that γH2AX appeared almost exclusively in the nuclei of etoposide or camptothecin treated cells (Fig. 6A, F). However, the effect of drugs on H2AX phosphorylation was significantly weaker in Jurkat.1A cells and occurred at a slower kinetic rate, even though H2AX expression levels in both cell lines were similar and were not altered by the drug treatment (Fig. 6B, G).

Western blot studies revealed that the majority of the PICOT proteins reside in the cytoplasm and that only a small amount was observed in the nuclear fraction (Fig. 6C, H, J). Immunoblot of histone H3 verified the relative purity of the nuclear fraction (Fig. 6D, K), and immunoblot of β-actin served as a marker for the cytosolic fraction (Fig. 6E, I, J). The latter results also validate that equal amounts of proteins were loaded per lane.

The retarded phosphorylation of H2AX in PICOT-deficient cells was induced by inhibitors of both topoisomerase I (camptothecin) and topoisomerase II (etoposide). This could imply that the PICOT-induced effects on H2AX phosphorylation were not dependent on the type of topoisomerase and/or restricted to DNA single- or double-strand breaks, but reflected the general drug-induced increase in intracellular ROS which promoted DNA damage [52–55].

To test this hypothesis, we used the well described antioxidant *N*-acetyl L-cysteine (NAC), which was administered to the cells prior to their treatment with etoposide. Nuclear fractions that were prepared from the cells at 1 h post etoposide treatment were subjected to SDS-PAGE and immunoblotting using anti-γH2AX Abs. The results (Fig. 7) demonstrated that the expression levels of nuclear γH2AX in etoposide-treated Jurkat T cells were significantly higher than those observed in the PICOT-deficient Jurkat.1A cells. However, the impact of the antioxidant, NAC, on the phosphorylation of H2AX in presence of etoposide was almost negligible in both cell lines. The results suggest that the impact of PICOT on etoposide-induced H2AX phosphorylation in Jurkat cells is not dependent on mechanisms which regulate the intracellular ROS.

3.6. Knockdown of PICOT results in decreased phosphorylation of the ATR, Chk1 and Chk2 serine/threonine kinases in response to etoposide

Phosphorylation and activation of H2AX and formation of γH2AX-containing foci at the DNA DSB sites occur within seconds following DSB [56]. The H2AX upstream serine/threonine kinases include the ATM (ataxia telangiectasia mutated), ATR (ATM and Rad3-related), and to a lesser degree, the phosphatidylinositol 3-kinases, DNA-PK (DNA-dependent protein kinase) [57]. Since many of the ATM and ATR functions are mediated by their downstream targets, the Chk1 and Chk2 serine/threonine kinases, we tested the effect of PICOT knockdown on the extent of phosphorylation and activation of these kinases in etoposide-treated cells.

Undetectable levels of phosphorylation of Chk1 on Ser-345 were observed in resting Jurkat and Jurkat.1A cells (Fig. 8A). One-hour treatment of cells with etoposide induced Chk1 phosphorylation on Ser-345, which peaked at 4 h. A similar time-dependent increase in phosphorylation of Chk1 was observed in the PICOT-deficient cells line, Jurkat.1A, except that the phosphorylation levels were ~2-fold lower than those in the wild type Jurkat. Chk1 expression levels were similar in both cell lines, and were not affected by the etoposide treatment (Fig. 8B).

Etoposide treatment of Jurkat cells had almost no effect on the

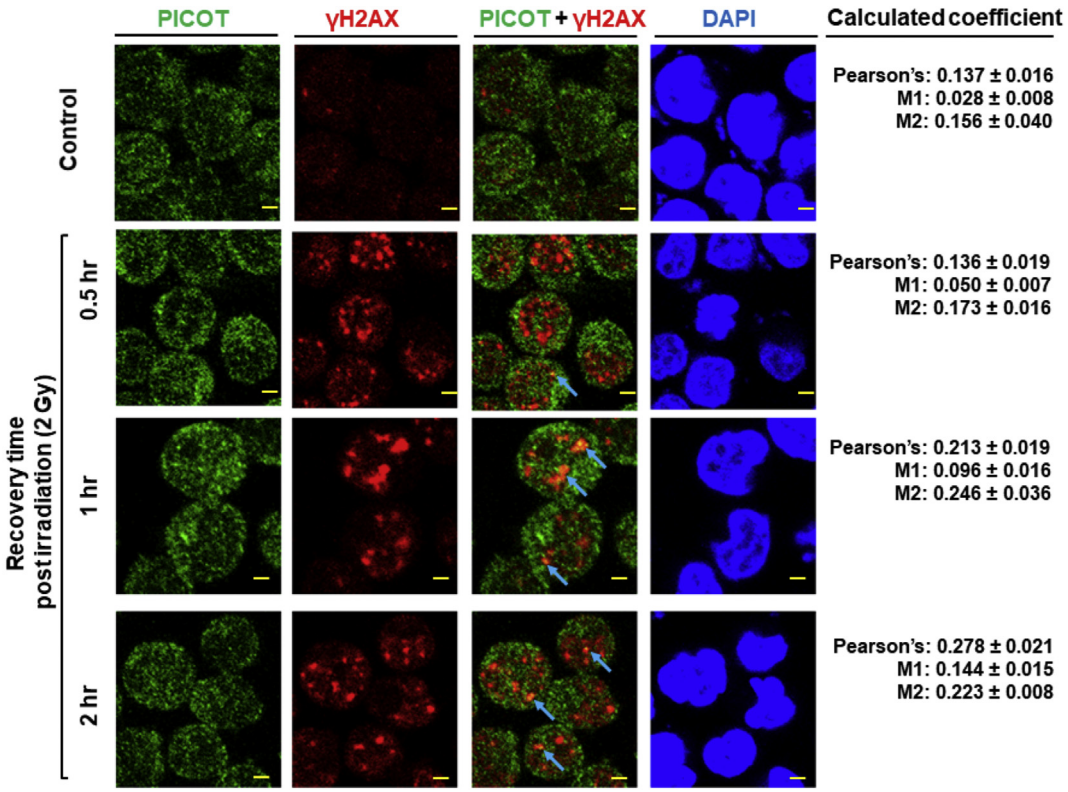

Fig. 5. PICOT partially colocalizes with nuclear γH2AX foci in X-ray irradiated Jurkat T cells.
A. Jurkat and Jurkat.1A cells (2×10^6/group) were irradiated with X-ray (2 Gy) and left to recover in vitro for the indicated time points at 37 °C in a 5% CO_2 incubator. The cells were then seeded on poly-L-lysine-coated slides and deposited by centrifugation. After fixation and permeabilization, the cells were incubated with mouse anti-PICOT and rabbit anti-γH2AX Abs, followed by staining with Cy3 (green)-conjugated goat anti-mouse and Cy5 (red)-conjugated goat anti-rabbit Ig Abs plus DAPI (blue). Cells were then analysed on an Olympus Fluoview 1000 laser scanning confocal microscope. Control treatments were performed using the same protocol with no irradiation. PICOT-γH2AX colocalization is demonstrated in a color overlay panel and areas of colocalization are marked by light blue arrows. Scale bar equals 2.5 μM. Pearson's coefficient and Mander's overlap coefficient were calculated on ~100 cells and average values ± standard deviation are included.

extent of phosphorylation of ATR-Ser-428 (Fig. 8C), although the phosphorylation was reduced by ~2-fold in Jurkat.1A cells. The expression levels of ATR were similar in both cell lines and were not affected by the etoposide treatment (Fig. 8D).

Numerical values of the Western blot data were obtained by measuring the intensity of the protein bands and presentation of the relative expression levels of the phosphoproteins in bar graphs (Fig. 8G, H).

Similar to its effect on Chk1, etoposide also induced the phosphorylation of Chk2 in both cell lines, even though the phosphorylation intensities were significantly weaker in Jurkat.1A cells at 4, 7, and 10 h post-treatment (Fig. 9A). The expression levels of Chk2 were similar in both cell lines and were unaffected by the etoposide treatment (Fig. 9B).

Finally, we measured the effect of etoposide on the phosphorylation of ATM. While ATM phosphorylation was also induced by etoposide, in contrast to the effect on the three former kinases, ATM phosphorylation was not inhibited, but slightly augmented, in PICOT-deficient Jurkat.1A cells (Fig. 9C). Considering the fact that the basal level of phosphorylated ATM in untreated cells was significantly higher in Jurkat.1A cells, the relative increase in phosphorylation in response to drug treatment was notably higher in Jurkat compared to Jurkat.1A cells (Fig. 9C,H). The relative intensities of the phosphoprotein bands were determined by densitometry and presented in a bar graph (Fig. 9G, H).

4. Discussion

PICOT was discovered in the year 2000 [23], and because of similarities in primary sequences and the 3-D conformations, it was assigned to the family of the glutaredoxins. Nevertheless, the physiological functions of PICOT in mammalian cells remain poorly understood and evidences for the glutaredoxin enzymatic activity of PICOT are still largely unknown.

In this study, we used Jurkat T cell sublines that stably expressed normal or reduced level of PICOT and tested the relevance of PICOT to cell survival in the presence of cytotoxic agents or X-ray irradiation.

Our studies demonstrated that partial depletion of PICOT in Jurkat T cells led to increased cell sensitivity to stress-inducing agents. We also observed that camptothecin and etoposide induced time- and concentration-dependent accumulation of very large DNA fragments in Jurkat cells, compared to a DNA 'ladders' in Jurkat.1A cells. While the large DNA fragments represent the early commitment of T cell to apoptosis [47] the DNA 'ladder' formed by integer multiples of ~200 bp oligonucleosomal size fragments represents a more advanced stage of the apoptotic process.

Additional studies revealed that PICOT is required for the normal maintenance of genome stability and that can indirectly contribute to the regulation of the ATR-Chk1/Chk2-γH2AX pathways which are critical for the stress-induced DNA-damage responses.

Recent studies demonstrated that PICOT alleviates myocardial ischemia-reperfusion injury by reducing intracellular levels of ROS [35], and other findings showed that PICOT knockdown in oral squamous cell carcinoma triggered the generation of ROS concomitant with a decrease in vitro cell migration and invasion [26]. These studies endorse the assumption that PICOT functions as an antioxidant enzyme that supports the maintenance of low intracellular levels of ROS, and thereby prevents ROS-induced damages to DNA and other cellular components. However, studies demonstrating that PICOT is overexpressed in nasopharyngeal carcinoma (NPC) indicates that the

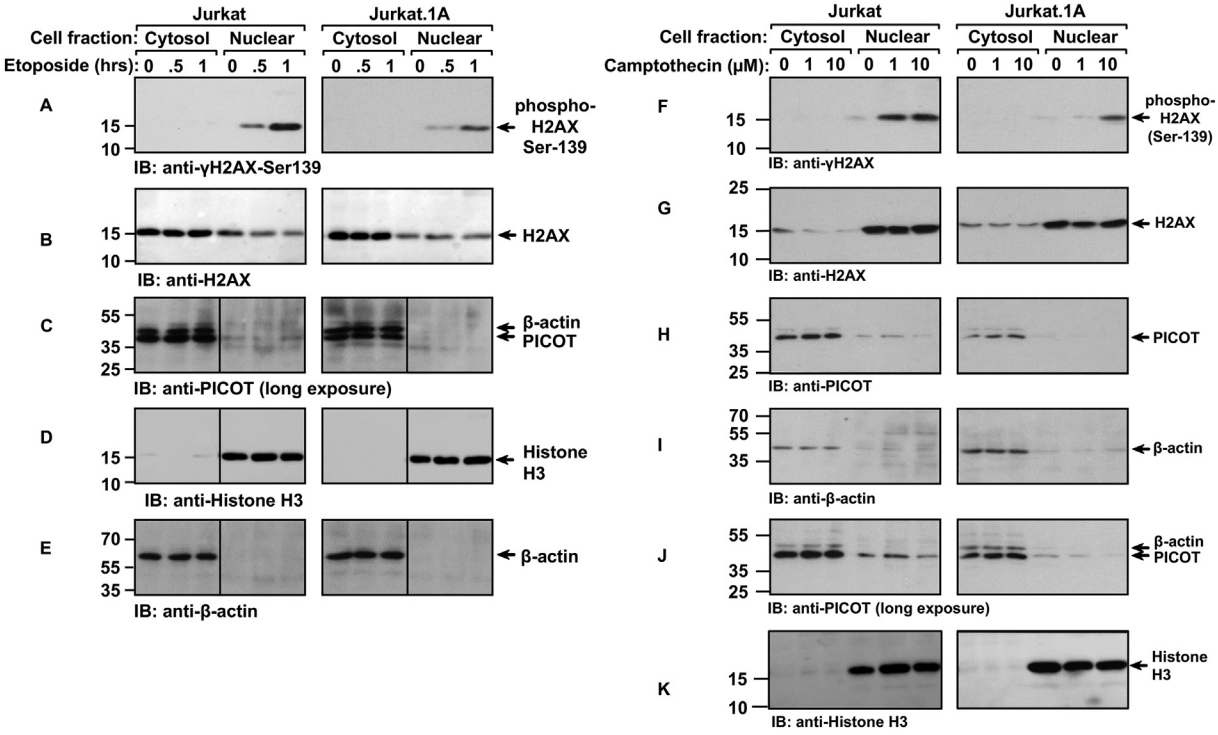

Fig. 6. Knockdown of PICOT results in decreased and delayed expression of nuclear γH2AX in camptothecin- and etoposide-treated Jurkat T cells.
Jurkat and Jurkat.1A T cells were treated with A. etoposide (30 μM) for different time intervals, or B. different concentration of camptothecin for 1 h, at 37 °C in a 5% CO_2 incubator. Cell lysates were separated into cytoplasmic and nuclear fractions and equivalent amounts of proteins (12.5 μg) were loaded per lane and subjected to SDS-PAGE on 12.5% acrylamide gels followed by electroblotting onto nitrocellulose membranes. Phospho-H2AX was visualized by membrane immunoblotting with rabbit polyclonal Abs directed against phospho-Ser139-H2AX (A, F). The membrane was stripped and sequentially immunoblotted with Abs specific for H2AX (B, G), PICOT (C, H), and β-actin (E, I), which was used to validate equal loading of cytoplasmic proteins. Equal loading of nuclear proteins was validated using Histone H3 specific Abs (D, K). Molecular weight markers (kDa) are indicated on the left and arrows mark the position of the indicated protein bands. Results are representative of three independent experiments. h, hours; IB, immunoblot.

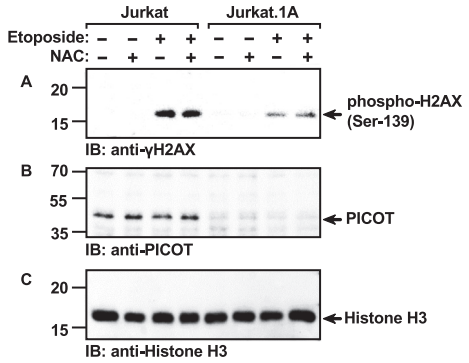

Fig. 7. The effect of PICOT on the induction of nuclear γH2AX expression in etoposide-treated cells is ROS independent.
(A). Jurkat and Jurkat.1A T cells were treated with *N*-acetyl L-cysteine (NAC; 5 mM) for 1 h, followed by treatment with etoposide (10 μM) for 1 h, at 37 °C in a 5% CO_2 incubator. Nuclear fractions (12.5 μg/ lane) were subjected to SDS-PAGE on 12.5% acrylamide gels and electroblotting onto nitrocellulose membranes. Phospho-H2AX was visualized by membrane immunoblotting with rabbit polyclonal Abs directed against phospho-Ser139-H2AX. The membrane was stripped and sequentially immunoblotted with Abs specific for PICOT (B), and histone H3 (C), to validate for equal loading of nuclear proteins. Molecular weight markers (kDa) are indicated on the left and arrows mark the position of the indicated protein bands. Results are representative of three independent experiments.

requirement for PICOT in the induction of in vitro proliferation and in vivo tumorigenesis of NPC cells, occurs independently of ROS production [30].

We found that partial depletion of PICOT in Jurkat T cell had no effect on the basal levels of intracellular ROS, but in response to hydrogen peroxide, ROS levels in PICOT-depleted cells were significantly higher than in wild type Jurkat. We assume that under normal conditions, activities of redox proteins, such as catalases and superoxide dismutases are sufficient for maintaining ROS homeostasis, while under acute stress conditions, the presence of PICOT might be essential for optimal maintenance of the basal levels of ROS.

In order to test the relevance of PICOT to genotoxic drug-induced cellular responses we treated Jurkat T cells with camptothecin or etoposide, two anti-cancer chemotherapeutic drugs that inhibit topoisomerase I and topoisomerase II respectively, and induce predominantly single- but also double-strand DNA breaks [58,59]. While both drugs induced a time- and concentration-dependent DNA fragmentation and promoted caspase-3 activity in Jurkat T cells, both phenomena were more prominent in the PICOT-deficient cells. Caspase-3 plays a central role in the execution-phase of cell apoptosis [48], and the increase in the extent of an active caspase-3 in PICOT-deficient cells correlates with the increased cell death. This direct correlation is not necessarily linear, since PICOT deficiency might also impact on other proteins, such as inhibitor-of-apoptosis (IAP) family members [60], and/or enzymes that modify caspase 3 post-translationally [61].

Since etoposide-induced cell apoptosis occurs concomitantly with the phosphorylation of the nuclear histone variant, H2AX [62], we tested whether PICOT might affect the extent of the drug-induced phosphorylation of H2AX, and further analysed whether such alteration might occur in the nucleus. We found that a partial depletion of PICOT in Jurkat T cells resulted in a delayed and reduced expression of γH2AX following cell treatment with either etoposide or camptothecin.

H2AX is a chromatin-bound histone [49] that plays a key role in the DNA damage repair mechanism, and is required for the preservation of

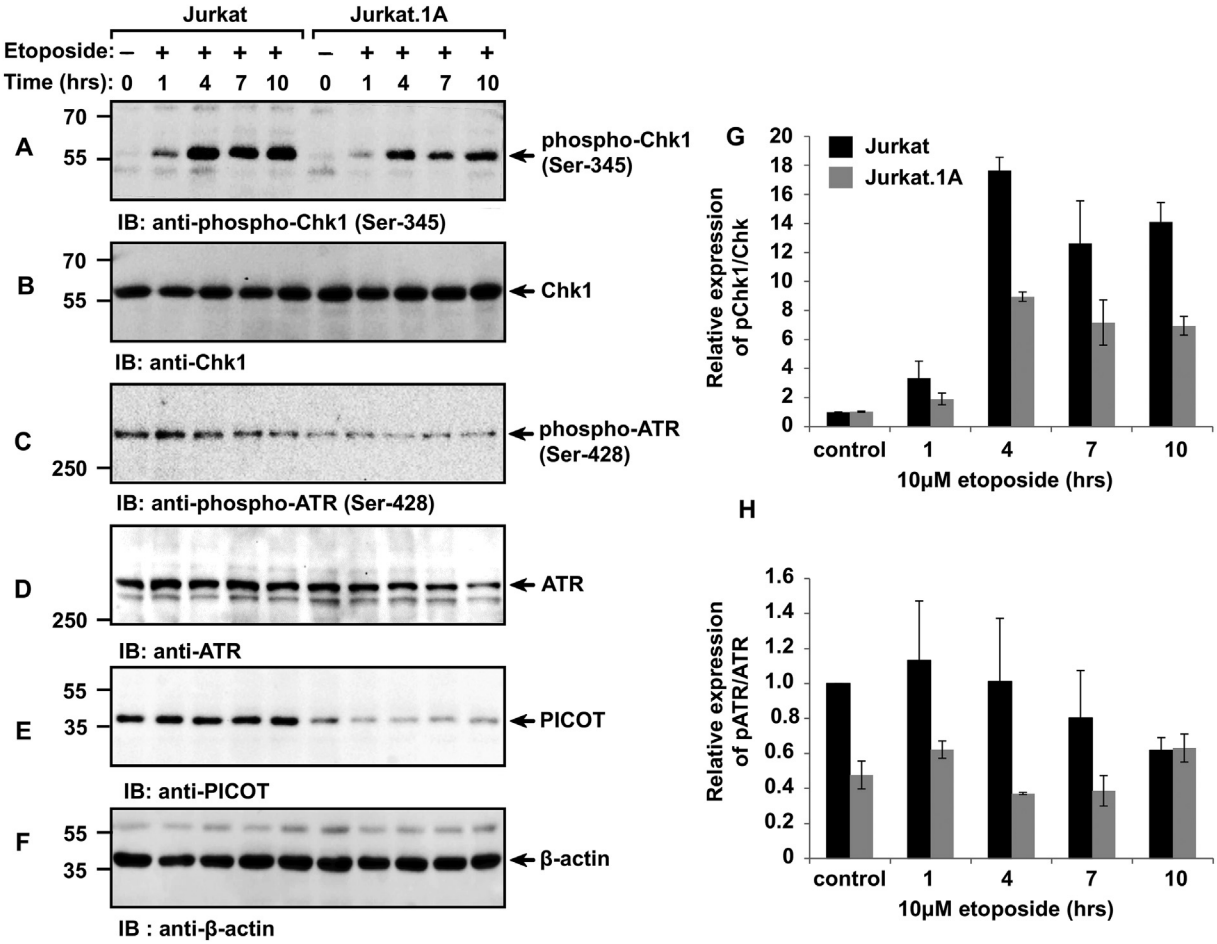

Fig. 8. Knockdown of PICOT results in inhibition of Chk1-Ser345 and ATR-Ser428 phosphorylation in response of Jurkat T cells to etoposide.
Jurkat and Jurkat.1A cells (5×10^6/group) were either not treated (−) or treated with 10 μM etoposide (+) for the indicated time intervals at 37 °C in a 5% CO_2. Whole cell lysates, equivalent to 20 μg proteins/lane (A, B, E, F) and 40 μg proteins/lane (C, D) were resolved by SDS-PAGE on 10% and 6.5% polyacrylamide gels, respectively. Proteins were then electroblotted onto nitrocellulose membranes which were incubated with anti-pChk1-Ser345 (A) or anti-Chk1 Abs (B), anti-pATR-Ser428 (C) or anti-ATR Abs (D) Comparison of PICOT expression levels in Jurkat and Jurkat.1A were performed using anti-PICOT mAbs (E), while immunoblot of β-actin served as a loading control (F). The relative intensity of protein band was determined using the *ImageJ* densitometry software and the relative expression of pChk1 vs. Chk1 and pATR vs. ATR was calculated and plotted as a bar graph for each time point (G, H). Bar graph represent the mean ± standard error of three independent experiments. The position of specific protein bands is indicated by arrows.

the cells' genomic integrity. Damage to DNA promotes the rapid phosphorylation of H2AX on Ser-139, which appears as discrete nuclear foci at the site of each nascent DSB, and operates as a platform for the recruitment of downstream mediators and chromatin modifying proteins [51].

The increased DNA fragmentation and the reduced H2AX phosphorylation in PICOT-deficient cells, in response to the DNA damage-inducing drugs, suggests that PICOT might be involved in the very early stages of the DDR.

Evaluation of γH2AX foci formation in irradiated cells is a well-known protocol for analyzing the early DNA damage response [51,63,64]. New γH2AX foci appear within minutes post cell irradiation, while their decline is considered as a marker for the DNA repair [49,65,66]. We found similar results in irradiated Jurkat T cells, where γH2AX foci were observed at 30 min post-irradiation. The lower level and the slower time-kinetic of γH2AX foci formation in irradiated PICOT-deficient cells suggested that PICOT has a positive contribution to the DDR. Moreover, immunofluorescence cell staining demonstrated partial colocalization of PICOT with γH2AX foci, suggesting that PICOT might affect some key players of DDR pathway.

Cellular induction of ROS in response to chemotherapeutic drugs, such as etoposide and camptothecin is one of several potential mechanisms that promote cell necrosis or apoptosis [67,68]. To test whether the contribution of PICOT to H2AX phosphorylation is ROS dependent, we treated Jurkat and Jurkat.1A cells with NAC, a thiol-containing antioxidant, which is widely used as a ROS scavenger [54,69,70]. We found that the level of etoposide-induced γH2AX expression in both Jurkat and Jurkat.1A cells was not altered by NAC treatment, suggesting that the effect of etoposide and the contribution of PICOT to γH2AX expression is ROS independent. Other studies have also demonstrated that etoposide-induced cell apoptosis may occur in the absence of ROS, via a caspase3/7-dependent pathway [54].

Phosphorylation of H2AX is mediated by upstream kinases that are members of the phosphotidyl-inositol-3-kinase (PI3K) family, and include the ATM, ATR, and to a lesser extent, the DNA-PK. These enzymes respond to DSB by phosphorylation of H2AX at ser-139, which currently serves as an indicator of DNA damage [71,72]. Upon the formation of γH2AX-containing foci at the DNA damage site, ATM and ATR further phosphorylate the Chk2 and Chk1 kinases, respectively [73]. These two enzymes, which play a pivotal role in maintaining the DNA integrity, further phosphorylate multiple substrates that regulate gene transcription, cell cycle progression, and apoptosis [74,75].

Our findings demonstrating that PICOT depletion downregulates ATR, Chk1 and Chk2 phosphorylation following Jurkat T cell exposure to etoposide suggest that PICOT might be required for the induction of very early steps following DSB (See Fig. 10).

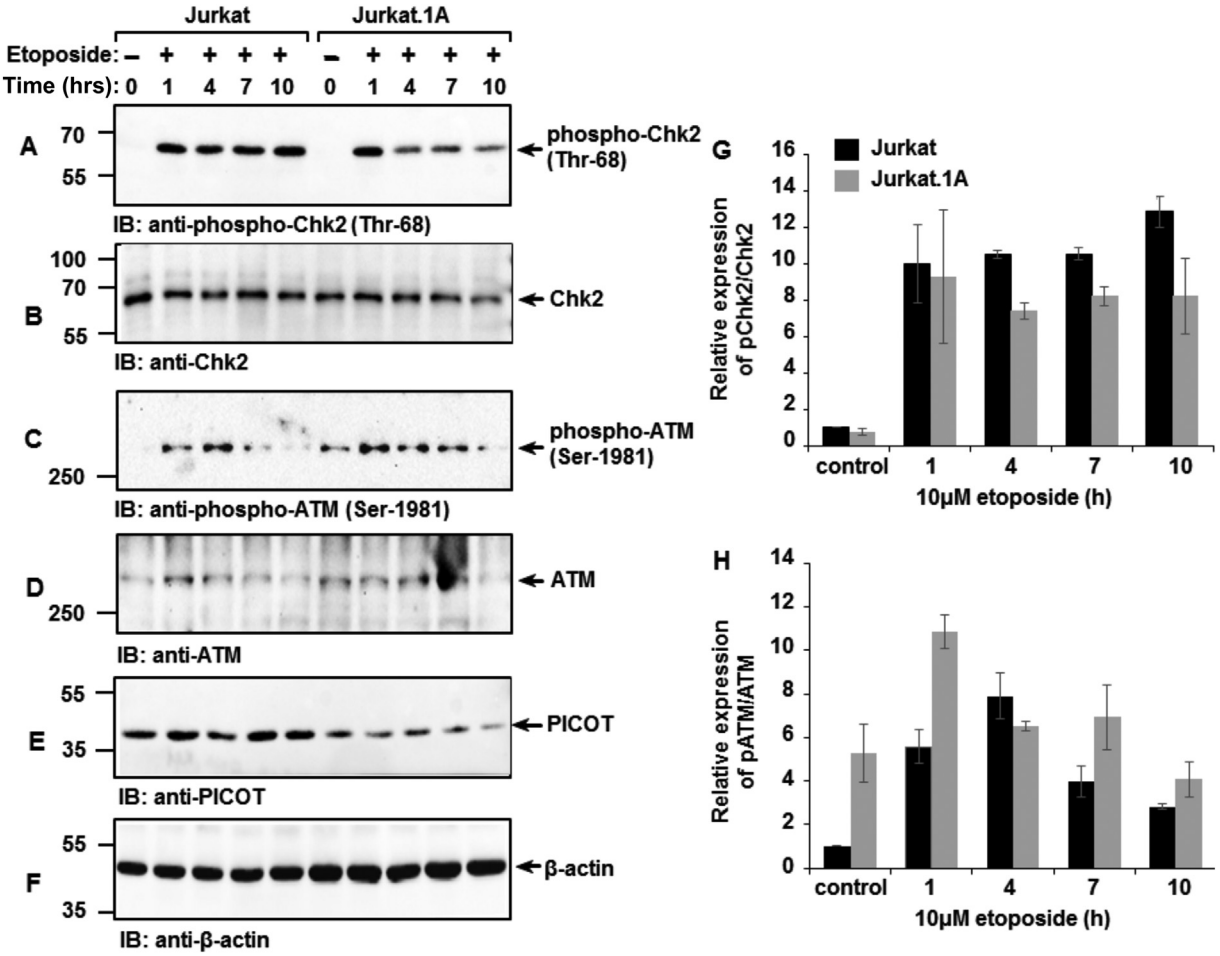

Fig. 9. Knockdown of PICOT results in downregulation of Chk2-Thr68- and upregulation of ATM-Ser1981- phosphorylation in response of Jurkat T cells to etoposide. Jurkat and Jurkat.1A cells (5×10^6/group) were left untreated (−) or treated with 10 μM etoposide (+) for indicated time intervals at 37 °C in a 5% CO_2 incubator. Whole cell lysates, equivalent to 20 μg (A, B, E, F) or 40 μg proteins/lane (C, D) were resolved by SDS-PAGE on 10% and 6.5% polyacrylamide gels, respectively. Proteins were then electroblotted onto nitrocellulose membranes which were incubated with anti-pChk2-Thr68 (A), anti-Chk2 (B), anti-pATM-Ser1981 (C), or anti-ATM Abs (D). Immunoblot of PICOT was used to verify the different PICOT expression level in Jurkat and Jurkat.1A (E). Immunoblot of β-actin served as a loading control (F). The relative intensity of protein bands was determined using the *ImageJ* densitometry software and the relative expression of pChk2 vs. Chk2 and pATR vs. ATR was calculated and plotted as a bar graph for each time points (G, H). Bar graph represent the mean ± standard error of three independent experiments. The position of specific protein bands is indicated by arrows.

The observation that phosphorylation of Chk2, but not ATM, is downregulated in PICOT-deficient cells is not expected considering the fact that a crosstalk exist between the ATM/CHK2 and ATR/CHK1 pathways [73,76], and the possibility that ATR might operate as an upstream kinase that phosphorylates both Chk1 and Chk2 in the etoposide/camptothecin-treated Jurkat cells. The ATM/CHK2 and ATR/CHK1 pathways are known to share multiple substrates, although they cannot compensate for the loss of each other [77,78].

ATR is also found in the cytosol where it plays an anti-apoptotic role in the mitochondria in response to UV damage [79]. However, this role is independent of its checkpoint/kinase activity and of its partner protein, ATR-interacting protein (ATRIP), which is required for sensing stress-induced DNA damages, activating DNA repair mechanisms and maintaining the DNA integrity [79,80]. Since ATR is an upstream regulator of Chk1 and H2AX, and phosphorylation of all three proteins is downregulated in PICOT-deficient cells, we hypothesize that PICOT might affect the activation state of the nuclear ATR and modulate the nuclear ATR-dependent checkpoint pathway.

While PICOT is considered an antioxidant enzyme, other potential regulatory activities of PICOT that may be involved in ATR-upstream events cannot be ruled out. For example, PICOT might affect ATR by physical interaction with and modulation of activity of proteins that regulate ATR activity, the location of ATR within the nucleus, or the availability of regulators required for the ATR-dependent DDR. The present findings suggest that the effect of PICOT on etoposide-induced DDR is ROS independent. Similar observations were made for the antioxidant enzyme, Nuclear factor erythroid 2-like 2 (Nrf2), which contributes to the radiation-induced DDR via a mechanism of homologous recombination and independent of ROS [81].

Since the DNA repair process involves multiple enzymes that reside or recruit to the γH2AX-containing foci, including 53BP1, MDC1, BMI1, Rad51 and other proteins [82–85], we intend to test the effect of PICOT on additional components of the DDR mechanism and test whether any of these proteins serves as a direct target for PICOT, which affect the entire process of the stress-induced DNA-damage response.

Disclosures

The authors have no financial conflicts of interest.

Acknowledgements

We thank Ms. Margalit Krup for her technical assistance, Ms. Caroline Simon and Ms. Judith Isakov for editorial assistance, and Dr.

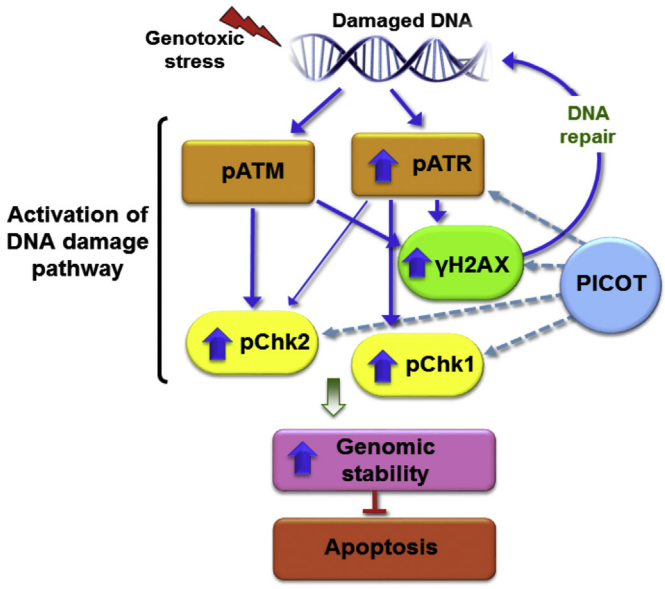

Fig. 10. Hypothetical model for the role of PICOT in T cells undergoing a genotoxic stress.

Mammalian cell exposure to a variety of genotoxic stress inducers (such as etoposide and camptothecin) result in double-strand DNA breaks (DSB). In response, the cells activate a complex network of stress response pathways collectively termed DNA damage response (DDR), which involves the rapid activation of multiple kinases and phosphorylation of substrate proteins. One of the best characterized events in the DSB repair response is the phosphorylation of the histone H2A variant, H2AX, on which is required for the DSB signaling response and for the retention of repair proteins at the DNA break sites.

Phospho-H2AX, termed γH2AX, in conjunction with additional nuclear proteins, promotes chromatin decondensation, which is essential for the DNA double-strand break repair, and might also contribute to the regulation of cell mitosis. Phosphorylation of H2AX on Ser139 is mediated by PI3-kinases, such as ATM and ATR, and is essential for the role of γH2AX in the DNA repair response. ATM and ATR undergo phosphorylation and activation in response to DSB and besides H2AX, phosphorylate additional downstream substrates, such as Chk1 and Chk2, respectively, which further phosphorylate substrate proteins that regulate gene transcription, cell cycle progression, and apoptosis. While the exact biological activities or the cellular target proteins of PICOT are not known, the present data suggest that PICOT plays a positive role in the DDR process and upregulates the phosphorylation of H2AX, apparently by activation of ATR. Thus, PICOT contributes to the increased genomic stability and consequently protect cells from stress induced apoptosis.

Ariel Ohayon for preparation of the PICOT-deficient Jurkat T cell sublines.

References

[1] P.D. Ray, B.W. Huang, Y. Tsuji, Reactive oxygen species (ROS) homeostasis and redox regulation in cellular signaling, Cell. Signal. 24 (2012) 981–990.
[2] G.S. Shadel, T.L. Horvath, Mitochondrial ROS signaling in organismal homeostasis, Cell 163 (2015) 560–569.
[3] A. Covarrubias, V. Byles, T. Horng, ROS sets the stage for macrophage differentiation, Cell Res. 23 (2013) 984–985.
[4] S. Chen, Y. Su, J. Wang, ROS-mediated platelet generation: a microenvironment-dependent manner for megakaryocyte proliferation, differentiation, and maturation, Cell Death Dis. 4 (2013) e722.
[5] Y.S. Bae, H. Oh, S.G. Rhee, Y.D. Yoo, Regulation of reactive oxygen species generation in cell signaling, Mol. Cell 32 (2011) 491–509.
[6] O. Sareila, T. Kelkka, A. Pizzolla, M. Hultqvist, R. Holmdahl, NOX2 complex-derived ROS as immune regulators, Antioxid. Redox Signal. 15 (2011) 2197–2208.
[7] P.A. Riley, Free radicals in biology: oxidative stress and the effects of ionizing radiation, Int. J. Radiat. Biol. 65 (1994) 27–33.
[8] Y. Yuan, S.H. Lee, S. Wu, The role of ROS in ionizing radiation-induced VLA-4 mediated adhesion of RAW264.7 cells to VCAM-1 under flow conditions, Radiat. Res. 179 (2013) 62–68.
[9] R. Kasiappan, S. Safe, ROS-inducing agents for cancer chemotherapy, Reactive Oxygen Species 1 (2016) 22–37.
[10] O.I. Aruoma, H. Kaur, B. Halliwell, Oxygen free radicals and human diseases, J. R. Soc. Health 111 (1991) 172–177.
[11] T. Yahata, T. Takanashi, Y. Muguruma, A.A. Ibrahim, H. Matsuzawa, T. Uno, Y. Sheng, M. Onizuka, M. Ito, S. Kato, K. Ando, Accumulation of oxidative DNA damage restricts the self-renewal capacity of human hematopoietic stem cells, Blood 118 (2011) 2941–2950.
[12] T. Hayashi, I. Hayashi, T. Shinohara, Y. Morishita, H. Nagamura, Y. Kusunoki, S. Kyoizumi, T. Seyama, K. Nakachi, Radiation-induced apoptosis of stem/progenitor cells in human umbilical cord blood is associated with alterations in reactive oxygen and intracellular pH, Mutat. Res. 556 (2004) 83–91.
[13] T. Yoshida, S. Goto, M. Kawakatsu, Y. Urata, T.S. Li, Mitochondrial dysfunction, a probable cause of persistent oxidative stress after exposure to ionizing radiation, Free Radic. Res. 46 (2012) 147–153.
[14] C.J. Doelman, A. Bast, Pro- and anti-oxidant factors in rat lung cytosol, Adv. Exp. Med. Biol. 264 (1990) 455–461.
[15] M. Rister, R.L. Baehner, The alteration of superoxide dismutase, catalase, glutathione peroxidase, and NAD(P)H cytochrome c reductase in Guinea pig polymorphonuclear leukocytes and alveolar macrophages during hyperoxia, J. Clin. Invest. 58 (1976) 1174–1184.
[16] A. Holmgren, Thioredoxin and glutaredoxin systems, J. Biol. Chem. 264 (1989) 13963–13966.
[17] J. Nordberg, E.S. Arner, Reactive oxygen species, antioxidants, and the mammalian thioredoxin system, Free Radical Biology & Medicine, vol. 31, 2001, pp. 1287–1312.
[18] C.H. Lillig, C. Berndt, A. Holmgren, Glutaredoxin systems, Biochim. Biophys. Acta 1780 (2008) 1304–1317.
[19] N. Isakov, S. Witte, A. Altman, PICOT-HD: a highly conserved protein domain that is often associated with thioredoxin and glutaredoxin modules, Trends Biochem. Sci. 25 (2000) 537–539.
[20] E. Herrero, M.A. de la Torre-Ruiz, Monothiol glutaredoxins: a common domain for multiple functions, Cell. Mol. Life Sci. 64 (2007) 1518–1530.
[21] Y. Babichev, S. Witte, A. Altman, N. Isakov, The Human PICOT Protein possesses a Thioredoxin-like Homology Domain and a Tandem repeat of a Novel Domain which is Highly Conserved during Evolution, IOS Press OHM, Amsterdam, Berlin, Oxford, Tokyo Washington, DC, 2001.
[22] N. Rouhier, J. Couturier, M.K. Johnson, J.P. Jacquot, Glutaredoxins: roles in iron homeostasis, Trends Biochem. Sci. 35 (2010) 43–52.
[23] S. Witte, M. Villalba, K. Bi, Y. Liu, N. Isakov, A. Altman, Inhibition of the c-Jun N-terminal kinase/AP-1 and NF-kappaB pathways by PICOT, a novel protein kinase C-interacting protein with a thioredoxin homology domain, J. Biol. Chem. 275 (2000) 1902–1909.
[24] N.H. Cheng, W. Zhang, W.Q. Chen, J. Jin, X. Cui, N.F. Butte, L. Chan, K.D. Hirschi, A mammalian monothiol glutaredoxin, Grx3, is critical for cell cycle progression during embryogenesis, FEBS J. 278 (2011) 2525–2539.
[25] H. Cha, J.M. Kim, J.G. Oh, M.H. Jeong, C.S. Park, J. Park, H.J. Jeong, B.K. Park, Y.H. Lee, D. Jeong, D.K. Yang, O.Y. Bernecker, D.H. Kim, R.J. Hajjar, W.J. Park, PICOT is a critical regulator of cardiac hypertrophy and cardiomyocyte contractility, J. Mol. Cell. Cardiol. 45 (2008) 796–803.
[26] B. Li, M. Chen, M. Lu, J. Xin-Xiang, P. Meng-Xiong, M. Jun-Wu, Glutaredoxin 3 promotes migration and invasion via the notch signalling pathway in oral squamous cell carcinoma, Free Radic. Res. 52 (2018) 390–401.
[27] D. Jeong, H. Cha, E. Kim, M. Kang, D.K. Yang, J.M. Kim, P.O. Yoon, J.G. Oh, O.Y. Bernecker, S. Sakata, T.T. Le, L. Cui, Y.H. Lee, D.H. Kim, S.H. Woo, R. Liao, R.J. Hajjar, W.J. Park, PICOT inhibits cardiac hypertrophy and enhances ventricular function and cardiomyocyte contractility, Circ. Res. 99 (2006) 307–314.
[28] A. Ohayon, Y. Babichev, R. Pasvolsky, G. Dong, I. Sztarkier, D. Benharroch, A. Altman, N. Isakov, Hodgkin's lymphoma cells exhibit high expression levels of the PICOT protein, J. Immunotoxicol. 7 (2010) 8–14.
[29] A. Ohayon, Y. Babichev, M. Galperin, A. Altman, N. Isakov, Widespread expression of PICOT in mouse and human tissues with predominant localization to epithelium, J. Histochem. Cytochem. 58 (2010) 799–806.
[30] F. He, L. Wei, W. Luo, Z. Liao, B. Li, X. Zhou, X. Xiao, J. You, Y. Chen, S. Zheng, P. Li, M. Murata, G. Huang, Z. Zhang, Glutaredoxin 3 promotes nasopharyngeal carcinoma growth and metastasis via EGFR/Akt pathway and independent of ROS, Oncotarget 7 (2016) 37000–37012.
[31] M.K. Cha, I.H. Kim, Preferential overexpression of glutaredoxin3 in human colon and lung carcinoma, Cancer Epidemiol. 33 (2009) 281–287.
[32] Y. Babichev, S. Gelkop, S. Witte, A. Altman, N. Isakov, The Protein Kinase C (PKC) theta-Interacting Proein, PICOT, undergoes Tyrosine Phosphorylation in Response to Hydrogen Peroxide, Monduzzi Editore, Bologna, Italy, 2000.
[33] Y. Babichev, N. Isakov, Tyrosine phosphorylation of PICOT and its translocation to the nucleus in response of human T cells to oxidative stress, Adv. Exp. Med. Biol. 495 (2001) 41–45.
[34] K. Pham, R. Pal, Y. Qu, X. Liu, H. Yu, S.L. Shiao, X. Wang, E. O'Brian Smith, X. Cui, G.G. Rodney, N. Cheng, Nuclear glutaredoxin 3 is critical for protection against oxidative stress-induced cell death, Free Radic. Biol. Med. 85 (2015) 197–206.
[35] J. Kim, J. Kim, H. Kook, W.J. Park, PICOT alleviates myocardial ischemia-reperfusion injury by reducing intracellular levels of reactive oxygen species, Biochem. Biophys. Res. Commun. 485 (2017) 807–813.
[36] P. Haunhorst, C. Berndt, S. Eitner, J.R. Godoy, C.H. Lillig, Characterization of the human monothiol glutaredoxin 3 (PICOT) as iron-sulfur protein, Biochem. Biophys. Res. Commun. 394 (2010) 372–376.
[37] H. Li, D.T. Mapolelo, S. Randeniya, M.K. Johnson, C.E. Outten, Human glutaredoxin 3 forms [2Fe-2S]-bridged complexes with human BolA2, Biochemistry 51 (2012) 1687–1696.
[38] P. Haunhorst, E.M. Hanschmann, L. Brautigam, O. Stehling, B. Hoffmann,

U. Muhlenhoff, R. Lill, C. Berndt, C.H. Lillig, Crucial function of vertebrate glutaredoxin 3 (PICOT) in iron homeostasis and hemoglobin maturation, Mol. Biol. Cell 24 (2013) 1895–1903.
[39] A.G. Frey, D.J. Palenchar, J.D. Wildemann, C.C. Philpott, A Glutaredoxin.BolA complex serves as an iron-sulfur cluster chaperone for the cytosolic cluster assembly machinery, J. Biol. Chem. 291 (2016) 22344–22356.
[40] J. Carmichael, W.G. Degraff, A.F. Gazdar, J.D. Minna, J.B. Mitchell, Evaluation of a tetrazolium-based semiautomated colorimetric assay - assessment of chemosensitivity testing, Cancer Res. 47 (1987) 936–942.
[41] H. Wang, J.A. Joseph, Quantifying cellular oxidative stress by dichlorofluorescein assay using microplate reader, Free Radical Bio Med 27 (1999) 612–616.
[42] B. Auer, H.P. Vosberg, U. Buhre, H. Klocker, M. Hirsch-Kauffmann, M. Schweiger, Intracellular distribution of DNA topoisomerase I in fibroblasts from patients with Fanconi's anaemia, Hum. Genet. 61 (1982) 369–371.
[43] S. Bolte, F.P. Cordelieres, A guided tour into subcellular colocalization analysis in light microscopy, J. Microsc. 224 (2006) 213–232.
[44] A.N. Sortibran, M.G. Tellez, R. Rodriguez-Arnaiz, Genotoxic profile of inhibitors of topoisomerases I (camptothecin) and II (etoposide) in a mitotic recombination and sex-chromosome loss somatic eye assay of Drosophila melanogaster, Mutat. Res. 604 (2006) 83–90.
[45] B.H. Long, S.T. Musial, M.G. Brattain, Single- and double-strand DNA breakage and repair in human lung adenocarcinoma cells exposed to etoposide and teniposide, Cancer Res. 45 (1985) 3106–3112.
[46] S.E. Porter, J.J. Champoux, The basis for camptothecin enhancement of DNA breakage by eukaryotic topoisomerase I, Nucleic Acids Res. 17 (1989) 8521–8532.
[47] G.M. Cohen, X.M. Sun, H. Fearnhead, M. MacFarlane, D.G. Brown, R.T. Snowden, D. Dinsdale, Formation of large molecular weight fragments of DNA is a key committed step of apoptosis in thymocytes, J. Immunol. 153 (1994) 507–516.
[48] S. Mazumder, D. Plesca, A. Almasan, Caspase-3 activation is a critical determinant of genotoxic stress-induced apoptosis, Methods Mol. Biol. 414 (2008) 13–21.
[49] E.P. Rogakou, D.R. Pilch, A.H. Orr, V.S. Ivanova, W.M. Bonner, DNA double-stranded breaks induce histone H2AX phosphorylation on serine 139, J. Biol. Chem. 273 (1998) 5858–5868.
[50] A. Sharma, K. Singh, A. Almasan, Histone H2AX phosphorylation: a marker for DNA damage, Methods Mol. Biol. 920 (2012) 613–626.
[51] E.P. Rogakou, C. Boon, C. Redon, W.M. Bonner, Megabase chromatin domains involved in DNA double-strand breaks in vivo, J. Cell Biol. 146 (1999) 905–916.
[52] N.A. Pham, D.W. Hedley, Respiratory chain-generated oxidative stress following treatment of leukemic blasts with DNA-damaging agents, Exp. Cell Res. 264 (2001) 345–352.
[53] A. Gorman, A. McGowan, T.G. Cotter, Role of peroxide and superoxide anion during tumour cell apoptosis, FEBS Lett. 404 (1997) 27–33.
[54] H.J. Shin, H.K. Kwon, J.H. Lee, M.A. Anwar, S. Choi, Etoposide induced cytotoxicity mediated by ROS and ERK in human kidney proximal tubule cells, Sci. Rep. 6 (2016) 34064.
[55] R.G. Jayasooriya, Y.H. Choi, J.W. Hyun, G.Y. Kim, Camptothecin sensitizes human hepatoma Hep3B cells to TRAIL-mediated apoptosis via ROS-dependent death receptor 5 upregulation with the involvement of MAPKs, Environ. Toxicol. Pharmacol. 38 (2014) 959–967.
[56] E. Markova, N. Schultz, I.Y. Belyaev, Kinetics and dose-response of residual 53BP1/gamma-H2AX foci: co-localization, relationship with DSB repair and clonogenic survival, Int. J. Radiat. Biol. 83 (2007) 319–329.
[57] S. Burma, B.P. Chen, M. Murphy, A. Kurimasa, D.J. Chen, ATM phosphorylates histone H2AX in response to DNA double-strand breaks, J. Biol. Chem. 276 (2001) 42462–42467.
[58] T. Yamauchi, A. Yoshida, T. Ueda, Camptothecin induces DNA strand breaks and is cytotoxic in stimulated normal lymphocytes, Oncol. Rep. 25 (2011) 347–352.
[59] A. Muslimovic, S. Nystrom, Y. Gao, O. Hammarsten, Numerical analysis of etoposide induced DNA breaks, PLoS One 4 (2009) e5859.
[60] Y. Shi, Caspase activation, inhibition, and reactivation: a mechanistic view, Protein Sci. 13 (2004) 1979–1987.
[61] A.V. Zamaraev, G.S. Kopeina, E.A. Prokhorova, B. Zhivotovsky, I.N. Lavrik, Post-translational modification of caspases: the other side of apoptosis regulation, Trends Cell Biol. 27 (2017) 322–339.
[62] T. Tanaka, H.D. Halicka, F. Traganos, K. Seiter, Z. Darzynkiewicz, Induction of ATM activation, histone H2AX phosphorylation and apoptosis by etoposide: relation to cell cycle phase, Cell Cycle 6 (2007) 371–376.
[63] A. Ivashkevich, C.E. Redon, A.J. Nakamura, R.F. Martin, O.A. Martin, Use of the gamma-H2AX assay to monitor DNA damage and repair in translational cancer research, Cancer Lett. 327 (2012) 123–133.
[64] O.A. Sedelnikova, E.P. Rogakou, I.G. Panyutin, W.M. Bonner, Quantitative detection of (125)IdU-induced DNA double-strand breaks with gamma-H2AX antibody, Radiat. Res. 158 (2002) 486–492.
[65] A. Kinner, W. Wu, C. Staudt, G. Iliakis, Gamma-H2AX in recognition and signaling of DNA double-strand breaks in the context of chromatin, Nucleic Acids Res. 36 (2008) 5678–5694.
[66] M. Lobrich, A. Shibata, A. Beucher, A. Fisher, M. Ensminger, A.A. Goodarzi, O. Barton, P.A. Jeggo, gammaH2AX foci analysis for monitoring DNA double-strand break repair: strengths, limitations and optimization, Cell Cycle 9 (2010) 662–669.
[67] J. Alexandre, F. Batteux, C. Nicco, C. Chereau, A. Laurent, L. Guillevin, B. Weill, F. Goldwasser, Accumulation of hydrogen peroxide is an early and crucial step for paclitaxel-induced cancer cell death both in vitro and in vivo, Int. J. Cancer 119 (2006) 41–48.
[68] D.R. Bickers, M. Athar, Oxidative stress in the pathogenesis of skin disease, J Invest Dermatol 126 (2006) 2565–2575.
[69] C.H. Ko, S.C. Shen, L.Y. Yang, C.W. Lin, Y.C. Chen, Gossypol reduction of tumor growth through ROS-dependent mitochondria pathway in human colorectal carcinoma cells, Int. J. Cancer 121 (2007) 1670–1679.
[70] M. Mayer, M. Noble, N-acetyl-L-cysteine is a pluripotent protector against cell death and enhancer of trophic factor-mediated cell survival in vitro, Proc. Natl. Acad. Sci. U. S. A. 91 (1994) 7496–7500.
[71] X. Huang, H.D. Halicka, Z. Darzynkiewicz, Detection of histone H2AX phosphorylation on Ser-139 as an indicator of DNA damage (DNA double-strand breaks), *Curr Protoc Cytom* Chapter 7 (2004) (Unit 7 27).
[72] T. Tanaka, A. Kurose, X. Huang, W. Dai, Z. Darzynkiewicz, ATM activation and histone H2AX phosphorylation as indicators of DNA damage by DNA topoisomerase I inhibitor topotecan and during apoptosis, Cell Prolif. 39 (2006) 49–60.
[73] J. Smith, L.M. Tho, N. Xu, D.A. Gillespie, The ATM-Chk2 and ATR-Chk1 pathways in DNA damage signaling and cancer, Adv. Cancer Res. 108 (2010) 73–112.
[74] H.C. Reinhardt, M.B. Yaffe, Kinases that control the cell cycle in response to DNA damage: Chk1, Chk2, and MK2, Curr. Opin. Cell Biol. 21 (2009) 245–255.
[75] Y. Chen, R.Y. Poon, The multiple checkpoint functions of CHK1 and CHK2 in maintenance of genome stability, Front. Biosci. 13 (2008) 5016–5029.
[76] T.P. Matthews, A.M. Jones, I. Collins, Structure-based design, discovery and development of checkpoint kinase inhibitors as potential anticancer therapies, Expert Opin. Drug Discovery 8 (2013) 621–640.
[77] K. Zaugg, Y.W. Su, P.T. Reilly, Y. Moolani, C.C. Cheung, R. Hakem, A. Hirao, Q. Liu, S.J. Elledge, T.W. Mak, Cross-talk between Chk1 and Chk2 in double-mutant thymocytes, Proc. Natl. Acad. Sci. U. S. A. 104 (2007) 3805–3810.
[78] L. Zannini, D. Delia, G. Buscemi, CHK2 kinase in the DNA damage response and beyond, J. Mol. Cell Biol. 6 (2014) 442–457.
[79] B.A. Hilton, Z. Li, P.R. Musich, H. Wang, B.M. Cartwright, M. Serrano, X.Z. Zhou, K.P. Lu, Y. Zou, ATR plays a direct Antiapoptotic role at mitochondria, which is regulated by Prolyl Isomerase Pin1, Mol. Cell 60 (2015) 35–46.
[80] D. Cortez, S. Guntuku, J. Qin, S.J. Elledge, ATR and ATRIP: partners in checkpoint signaling, Science 294 (2001) 1713–1716.
[81] S. Jayakumar, D. Pal, S.K. Sandur, Nrf2 facilitates repair of radiation induced DNA damage through homologous recombination repair pathway in a ROS independent manner in cancer cells, Mutat. Res. 779 (2015) 33–45.
[82] J. Suchankova, S. Kozubek, S. Legartova, P. Sehnalova, T. Kuntziger, E. Bartova, Distinct kinetics of DNA repair protein accumulation at DNA lesions and cell cycle-dependent formation of gammaH2AX- and NBS1-positive repair foci, Biol. Cell. 107 (2015) 440–454.
[83] M.T. Mok, B.R. Henderson, The in vivo dynamic interplay of MDC1 and 53BP1 at DNA damage-induced nuclear foci, Int. J. Biochem. Cell Biol. 44 (2012) 1398–1409.
[84] M.T. Mok, B.R. Henderson, Three-dimensional imaging reveals the spatial separation of gammaH2AX-MDC1-53BP1 and RNF8-RNF168-BRCA1-a complexes at ionizing radiation-induced foci, Radiother. Oncol. 103 (2012) 415–420.
[85] J. Reindl, S. Girst, D.W. Walsh, C. Greubel, B. Schwarz, C. Siebenwirth, G.A. Drexler, A.A. Friedl, G. Dollinger, Chromatin organization revealed by nanostructure of irradiation induced gammaH2AX, 53BP1 and Rad51 foci, Sci. Rep. 7 (2017) 40616.